Nonspectral Dirac random-phase approximation for finite nuclei

J. R. Shepard and E. Rost
Department of Physics, University of Colorado, Boulder, Colorado 80309

J. A. McNeil
Department of Physics, Colorado School of Mines, Golden, Colorado 80401
(Received 18 January 1989)

We present a version of the random-phase approximation for the description of nuclear excitations which is a consistent extension of the QHD1 mean-field theory of the ground states of doubly magic nuclei. This approach includes correlations induced by the isoscalar σ and ω mesons of QHD1. Our method employs a nonspectral single particle propagator in such a way that we avoid any basis truncation and automatically include the escape widths implied by the theory. Our calculations yield exactly conserved random-phase approximation transition currents as well as correct treatment of spuriosity for $1^- T=0$ excitations. Because of the flexibility of our numerical method, we can treat discrete excitations, giant resonances, and the continuum response in general—including quasielastic scattering—in a unified way. We compare our results with experimental (e,e') form factors for various discrete excitations in ^{12}C, ^{16}O, ^{40}Ca, and ^{48}Ca as well as with the quasielastic Coulomb response functions for ^{12}C and ^{40}Ca. Agreement with transition charge densities is typically quite good and in some cases superior to comparable nonrelativistic random-phase approximation calculations. Transition current densities are less well described. The question of sum rules in the relativistic random-phase approximation is also addressed.

I. INTRODUCTION

The QHD1 mean-field theory (MFT) of the ground states of doubly magic nuclei has been extensively studied[1,2] and has been found to reproduce experimental quantities like valence state binding energies and ground state charge distributions quite accurately with a minimum number of free parameters. In this paper, we discuss a consistent extension of the QHD1 MFT which accounts for one-particle, one-hole ($1p$-$1h$) excitations of the doubly magic nuclei. This extension is the MFT random-phase approximation (MFT RPA) which, on the basis of a long history of studies of the nonrelativistic RPA (see e.g., Refs. 3–6), we expect to provide especially good descriptions of low-lying collective excitations. Various versions of the MFT RPA applied to particular types of excitations have been discussed by other authors.[7–11] In the present work, we formulate a nonspectral version of the MFT RPA which avoids approximations intrinsic to the more common spectral approaches[7–10] and which allows a unified description of both discrete and continuum excitations with realistic boundary conditions for the latter.[11] We show MFT-RPA results for a number of discrete excitations in ^{12}C, ^{16}O, ^{40}Ca, and ^{48}Ca with special emphasis on electromagnetic properties. We also briefly discuss giant resonance phenomena as well as the quasielastic (e,e') Coulomb response.

II. REVIEW OF QHD1 MEAN-FIELD THEORY

In the QHD1 MFT of finite nuclei,[2] one begins with a Lagrangian density

$$\mathcal{L}=\mathcal{L}(\psi,\phi,V^\mu) \tag{2.1}$$

which specifies the behavior of interacting nucleon and isoscalar scalar (σ) and vector (ω) meson fields represented by ψ, ϕ, and V^μ, respectively. The interacting single particle Green function is obtained in Hartree approximation by summing tadpole diagrams:[1,2]

$$\begin{aligned} G(x,y)&=-\iota\langle\Psi_0|T[\hat{\psi}'(x)\hat{\bar{\psi}}'(y)]|\Psi_0\rangle \\ &\simeq G_H(x,y) \\ &=-\iota\langle\Phi_0|T[\hat{\psi}(x)\hat{\bar{\psi}}(y)]|\Phi_0\rangle \\ &=G_0(x,y)+\int d^4z\, G_0(x,z)\Sigma_H(z)G_H(z,y) \end{aligned} \tag{2.2}$$

with

$$\begin{aligned} \Sigma_H&=\Sigma_s+\gamma_\mu\Sigma_v^\mu\ , \\ \Sigma_s&=-\iota g_s^2\Delta_0\mathrm{Tr}(G_H)\ , \\ \Sigma_v^\mu&=+\iota g_v^2 D_0\mathrm{Tr}(\gamma^\mu G_H)\ , \end{aligned} \tag{2.3}$$

where G, G_0, and G_H are the full, free, and Hartree propagators, respectively, Ψ_0 (Φ_0) is the full (Hartree) ground state, and $\hat{\psi}'$ ($\hat{\psi}$) is the full (Hartree) field operator. Also, Σ_H is the Hartree self-energy consisting of scalar (Σ_s) and vector (Σ_v^μ) contributions depending on the scalar and vector coupling constants, g_s and g_v, respectively, and the meson propagators Δ_0 and D_0. In the MFT used here, the self-energies are evaluated subject to a further approximation which can be understood from the structure of G_H and will be discussed later in this section. The

Hartree basis consists of eigenfunctions of the following Dirac equation:

$$[\gamma^0\epsilon_\beta+\iota\boldsymbol{\gamma}\cdot\boldsymbol{\nabla}-m-\Sigma_s(r)-\gamma^0\Sigma_v^0(r)]\psi_\beta(\mathbf{r})=0 \tag{2.4}$$

where we have used the fact that, for doubly closed-shell nuclei, $\Sigma_v^\mu\rightarrow\Sigma_v^\mu\delta^{\mu,0}$; i.e., only the timelike component of Σ_v^μ is nonvanishing in the nuclear rest frame. This implies the eigenfunctions have total angular momentum as a good quantum number. We may express G_H in terms of the basis $\{\psi_\beta\}$ via a "spectral" expansion:

$$G_H(\mathbf{x},\mathbf{y};\omega)=\sum_\beta \psi_\beta(\mathbf{x})\bar{\psi}_\beta(\mathbf{y})G_\beta(\omega)$$

where

$$\begin{aligned}G_\beta(\omega)&=\left[\frac{\theta(\epsilon_\beta)}{\omega-\epsilon_\beta+\iota\eta}+\frac{\theta(-\epsilon_\beta)}{\omega-\epsilon_\beta-\iota\eta}\right]\\&\quad+2\pi\iota\delta(\omega-\epsilon_\beta)\theta(\epsilon_F-\epsilon_\beta)\theta(\epsilon_\beta)\\&=G_{V,\beta}(\omega)+G_{D,\beta}(\omega)\ .\end{aligned} \tag{2.5}$$

In these expressions, β labels a Hartree basis state, F represents the Fermi surface, and the structure of the vacuum contribution, $G_{V,\beta}$ ensures positive energy states propagate forward in time while negative energies go backward. The density contribution $G_{D,\beta}$ represents the correction due to the fact that positive-energy levels up to and including $\beta=F$ are occupied and should propagate backward, too. The self-energies of Eq. (2.3) are divergent due to the vacuum contributions entering via $G_{V,\beta}$ and vacuum polarization contributions can be computed only after a renormalization program is carried out.[2] The resulting theory is referred to as the relativistic hartree approximation (RHA). In the QHD1 MFT, however, the effect of the vacuum is assumed to be incorporated in the effective masses and coupling constants of the original Lagrangian density. We then explicitly treat only the contributions to Σ_H arising from $G_{D,\beta}$. Thus $\Sigma_H\rightarrow\Sigma_{\rm MF}$ where the scalar and vector terms of $\Sigma_{\rm MF}$ are defined as in Eq. (2.3), but with $G_H\rightarrow G_D$. The basis states are again eigenfunctions of Eq. (2.4) but with $\Sigma\rightarrow\Sigma_{\rm MF}$. In all calculations to be presented below, unless otherwise specified, we use the so-called "finite Hartree" coupling constants and meson masses given in Table V of Ref. 2.

In closing this section, we present an alternative "nonspectral" representation of the MFT propagator which appears in "spectral" form in Eq. (2.5). In a partial-wave expansion we write

$$\begin{aligned}G_{\rm MF}(\mathbf{x},\mathbf{y};\omega)=\sum_{ljm}[&\psi_{\mathrm{u};ljm}(\mathbf{x};\omega)\bar{\psi}_{\mathrm{v};ljm}(\mathbf{y};\omega)\theta(y-x)\\&+\psi_{\mathrm{v};ljm}(\mathbf{x};\omega)\bar{\psi}_{\mathrm{u};ljm}(\mathbf{y};\omega)\theta(x-y)]\end{aligned} \tag{2.6}$$

where $\psi_{\rm u}$ and $\psi_{\rm v}$ each satisfy Eq. (2.4) with $\epsilon_\beta\rightarrow\omega$ but where $\psi_{\rm u}$ ($\psi_{\rm v}$) is regular at $r=0(\infty)$ and where a suitable normalization is obtained by dividing by the Wronskian of the functions associated with the upper components of $\psi_{\rm u}$ and $\psi_{\rm v}$. Note that the linear independence of $\psi_{\rm u}$ and $\psi_{\rm v}$ is equivalent to specifying that ω is *not* an eigenvalue of Eq. (2.4). The details of the construction of this propagator are presented in Ref. 12 and in Appendix B. This "nonspectral" propagator can be thought of as a summation of the spectral form.

III. FORMALISM FOR QHD1-MFT RPA

There are numerous techniques for deriving the RPA equations for nuclear excitations beginning with the MFT ground state.[3–6] In order to be as consistent as possible with the treatment of the QHD1-MFT problem outlined above, we employ the Feynman rules of QHD1.[2]

We first consider some general properties of the fully interacting polarization insertion defined by

$$\begin{aligned}-\iota\Pi^{ij;kl}(x,y)&\\\equiv\langle\Psi_0|T[\hat{\psi}'^i(x)\hat{\bar{\psi}}'^j(x)\hat{\psi}'^k(y)\hat{\bar{\psi}}'^l(y)]|\Psi_0\rangle&\end{aligned} \tag{3.1}$$

where i, j, k, and l are Dirac indices. This object describes the propagation of a particle-hole excitation in the ground state of the fully interacting system just as G defined in Eq. (2.2) describes the propagation of a single particle (or hole). We may go over to the Lehmann representation,[6]

$$-\Pi(\mathbf{x},\mathbf{y};\omega)=\sum_n\left[\frac{\langle\Psi_0|\hat{\psi}'_S(\mathbf{x})\hat{\bar{\psi}}'_S(\mathbf{x})|\Psi_n\rangle\langle\Psi_n|\hat{\psi}'_S(\mathbf{y})\hat{\bar{\psi}}'_S(\mathbf{y})|\Psi_0\rangle}{\omega-\omega_n+\iota\eta}-\frac{\langle\Psi_0|\hat{\psi}'_S(\mathbf{y})\hat{\bar{\psi}}'_S(\mathbf{y})|\Psi_n\rangle\langle\Psi_n|\hat{\psi}'_S(\mathbf{x})\hat{\bar{\psi}}'_S(\mathbf{x})|\Psi_0\rangle}{\omega+\omega_n-\iota\eta}\right] \tag{3.2}$$

where Ψ_n is the full wave function for the nth excited state whose excitation energy is $\omega_n=E_n-E_0$ and where $\hat{\psi}'_S(\mathbf{x})$ is the full field operator in the Schrödinger picture. Evidently, Ψ_n must be, at least in part, a one-particle one-hole state with respect to the ground state. Other excited states make no contribution to Π. Equation (3.2) makes it clear that $\Pi(\mathbf{x},\mathbf{y};\omega)$ has poles at $\omega=\omega_n$ and that the residue (for $\omega>0$) is the outer product of the configuration space transition densities:

$$-\Pi(\mathbf{x},\mathbf{y};\omega\rightarrow\omega_n+\iota\eta)=\frac{\bar{\mathcal{F}}^{(n)}(\mathbf{x})\mathcal{F}^{(n)}(\mathbf{y})}{\iota\eta} \tag{3.3}$$

where

$$\mathcal{F}^{(n)}(\mathbf{y})\equiv\langle\Psi_n|\hat{\psi}'_S(\mathbf{y})\hat{\bar{\psi}}'_S(\mathbf{y})|\Psi_0\rangle \tag{3.4}$$

and where

$$\bar{\mathcal{F}}\equiv\gamma^0\mathcal{F}^\dagger\gamma^0\ .$$

According to the Feynman rules, the transition amplitude for an interaction having a vertex $\mathcal{O}$ can be expressed as

$$\langle \mathcal{O} \rangle^{(n)} = \int d^3y \, \mathrm{Tr}[\mathcal{O}(\mathbf{y})\mathcal{F}^{(n)}(\mathbf{y})] \tag{3.5}$$

where the trace is over Dirac indices. (See Appendix C for a more detailed discussion of $\langle \mathcal{O} \rangle^{(n)}$.) In a somewhat more general way, linear response theory[5,6] gives the response to an external probe whose interaction is represented by $\mathcal{O}$ as

$$S_{\mathcal{O}}(\omega) = -\frac{1}{\pi} \mathrm{Im} \int d^3x \, d^3y \, \mathrm{Tr}[\mathcal{O}(\mathbf{x})\Pi_{\mathrm{ret}}(\mathbf{x},\mathbf{y};\omega)\mathcal{O}(\mathbf{y})] \tag{3.6}$$

where Π_{ret} is the retarded[6] (or causal) version of Π. From Eqs. (3.2)–(3.6), we have

$$S_{\mathcal{O}}(\omega) = \sum_n |\langle \mathcal{O} \rangle^{(n)}|^2 [\delta(\omega-\omega_n) - \delta(\omega+\omega_n)] \, . \tag{3.7}$$

The standard techniques of field theory may be used to expand Π in terms of Hartree propagators and meson interactions. Retaining only the "ring" contributions and summing to all orders yields the following RPA integral equation:

$$\begin{aligned} -\iota\Pi^{ij;kl}(\mathbf{x},\mathbf{y};\omega) &\simeq -\iota\Pi^{ij;kl}_{\mathrm{RPA}}(\mathbf{x},\mathbf{y};\omega) \\ &= -\iota\Pi^{ij;kl}_{H}(\mathbf{x},\mathbf{y};\omega) + \sum_{\substack{mm' \\ nn'}} \int d^3x_1 d^3x_2 (-\iota)\Pi^{ij;mm'}_{H}(\mathbf{x},\mathbf{x}_1;\omega) \\ &\quad \times \sum_N (\Gamma^a_N)^{m'm} \iota D^0_{N;ab}(\mathbf{x}_1-\mathbf{x}_2;\omega)(\Gamma^b_N)^{n'n}(-\iota)\Pi^{nn';kl}_{\mathrm{RPA}}(\mathbf{x}_2,\mathbf{y};\omega) \end{aligned} \tag{3.8}$$

where N represents the meson type, a and b refer to; e.g., Lorentz indices, and m, m', etc. refer to Dirac indices. Also, Γ^a_N is a meson-NN vertex and $D^0_{N;ab}$ is the configuration space form of the free meson propagator. These quantities are discussed in detail in Appendix B. Finally, the Hartree polarization insertion is

$$-\iota\Pi^{ij;kl}_{H}(x,y) \equiv \langle \Phi_0 | T[\hat{\psi}^i(x)\hat{\bar{\psi}}^j(x)\hat{\psi}^k(y)\hat{\bar{\psi}}^l(y)] | \Phi_0 \rangle \tag{3.9}$$

or

$$-\iota\Pi^{ij;kl}_{H}(\mathbf{x},\mathbf{y};\omega) = \int \frac{d\omega'}{2\pi} G^{il}_{H}(\mathbf{x},\mathbf{y};\omega+\omega')G^{kj}_{H}(\mathbf{y},\mathbf{x};\omega') \, . \tag{3.10}$$

Using the spectral form for G_H given in Eq. (2.5), we have

$$-\iota\Pi^{ij;kl}_{H}(\mathbf{x},\mathbf{y};\omega) = \sum_{\alpha,\beta} \psi^i_\alpha(\mathbf{x})\bar{\psi}^l_\alpha(\mathbf{y})\psi^k_\beta(\mathbf{y})\bar{\psi}^j_\beta(\mathbf{x}) \, \iota \int \frac{d\omega'}{2\pi} G_\alpha(\omega+\omega')G_\beta(\omega') \, . \tag{3.11}$$

Again using Eq. (2.5), we have

$$G_\alpha(\omega+\omega')G_\beta(\omega') = (G_{V,\alpha}+G_{D,\alpha})(G_{V,\beta}+G_{D,\beta}) \, . \tag{3.12}$$

In keeping with the mean-field approximation, discussed in the preceding section, we drop the $G_{V,\alpha}G_{V,\beta}$ or "vacuum-vacuum" terms, retaining only the density-dependent contributions. This *defines* the mean-field polarization insertion:

$$\begin{aligned} -\iota\Pi^{ij;kl}_{\mathrm{MF}}(\mathbf{x},\mathbf{y};\omega) &\equiv \sum_{\alpha,\beta} \psi^i_\alpha(\mathbf{x})\bar{\psi}^l_\alpha(\mathbf{y})\psi^k_\beta(\mathbf{y})\bar{\psi}^j_\beta(\mathbf{x}) \\ &\quad \times \iota \int \frac{d\omega'}{2\pi} [G_{V,\alpha}(\omega+\omega')G_{D,\beta}(\omega') + G_{D,\alpha}(\omega+\omega')G_{V,\beta}(\omega') + G_{D,\alpha}(\omega+\omega')G_{D,\beta}(\omega')] \, . \end{aligned} \tag{3.13}$$

This approximation again assumes that vacuum polarization effects are accounted for in the phenomenological masses and coupling constants determined in the QHD1-MFT description of the ground state as discussed in the preceding section. In the full Hartree approximation, the divergent vacuum-vacuum contributions contained in the "$G_V G_V$" term are rendered finite by counterterm contributions determined in the renormalization program. A thorough discussion of this problem in the context of nuclear matter is given by Chin.[13]

The real and imaginary parts of Π_{MF} [Eq. (3.13)] are readily determined by performing the simple integrals over ω'. The result is

$$-\iota\Pi^{ij;kl}_{\mathrm{MF}}(\mathbf{x},\mathbf{y};\omega) = \iota \sum_{F \geq \beta > 0} \sum_{\substack{\alpha > F \\ \alpha < 0}} \left[\frac{\psi^i_\alpha(\mathbf{x})\bar{\psi}^j_\beta(\mathbf{x})\psi^k_\beta(\mathbf{y})\bar{\psi}^l_\alpha(\mathbf{y})}{\omega-\omega_{\alpha\beta}+\iota\eta(\alpha)} - \frac{\psi^i_\beta(\mathbf{x})\bar{\psi}^j_\alpha(\mathbf{x})\psi^k_\alpha(\mathbf{y})\bar{\psi}^l_\beta(\mathbf{y})}{\omega+\omega_{\alpha\beta}-\iota\eta(\alpha)} \right] , \tag{3.14}$$

where $\eta(\alpha) = +|\eta|$ for $\alpha > F$, $\eta(\alpha) = -|\eta|$ for $\alpha < 0$, and $\omega_{\alpha\beta} \equiv \epsilon_\alpha - \epsilon_\beta$. The causal or retarded version of Π_{MF} has positive infinitesimals in both terms on the right-hand side of Eq. (3.14). Defining $\tilde{\omega} \equiv \omega + \iota\eta$,

$$-\iota\Pi^{ij;kl}_{\mathrm{MF,ret}}(\mathbf{x},\mathbf{y};\omega)=-\iota\Pi^{ij;kl}_{\mathrm{MF}}(\mathbf{x},\mathbf{y};\tilde{\omega})$$
$$=\iota\sum_{\substack{F\geq\beta\\ \alpha}}\left[\frac{\psi^i_\alpha(\mathbf{x})\bar{\psi}^j_\beta(\mathbf{x})\psi^k_\beta(\mathbf{y})\bar{\psi}^l_\alpha(\mathbf{y})}{\tilde{\omega}-\omega_{\alpha\beta}}-\frac{\psi^i_\beta(\mathbf{x})\bar{\psi}^j_\alpha(\mathbf{x})\psi^k_\alpha(\mathbf{y})\bar{\psi}^l_\beta(\mathbf{y})}{\tilde{\omega}+\omega_{\alpha\beta}}\right], \tag{3.15}$$

where we have used the antisymmetry of the quantity in large parentheses for $\alpha\leftrightarrow\beta$ to include terms involving $F\geq\alpha>0$. Again using Eq. (2.5), we may perform the α sum. Dropping the ret subscript, we have

$$-\iota\Pi^{ij;kl}_{\mathrm{MF}}(\mathbf{x},\mathbf{y};\tilde{\omega})=\iota\sum_{F\geq\beta>0}[\psi^i_\beta(\mathbf{x})\bar{\psi}^l_\beta(\mathbf{y})G^{kj}_{\mathrm{MF}}(\mathbf{y},\mathbf{x};\epsilon_\beta-\tilde{\omega})+G^{il}_{\mathrm{MF}}(\mathbf{x},\mathbf{y};\epsilon_\beta+\tilde{\omega})\psi^k_\beta(\mathbf{y})\bar{\psi}^j_\beta(\mathbf{x})]\ . \tag{3.16}$$

As will be discussed in Sec. V, our calculational scheme stipulates that Π_{MF} and its RPA analogue are evaluated at $\tilde{\omega}=\omega+\iota\eta$, $\eta\simeq 0.1$ MeV, so that we always evaluate the *causal* polarization insertions as required by linear response theory [Eqs. (3.6) and (3.7)]. This will be important when sum rules are discussed in Sec. VII.

The QHD1-MFT RPA as outlined above is a consistent extension of the MFT description of the ground state to $1p$-$1h$ excitations based on that ground state. The consistency of the treatment has several interesting consequences. For example, the stability condition for the mean-field ground state also ensures real RPA excitation energies.[4] Conversely, imaginary RPA energies imply an unstable ground state. Consistency is also essential to ensure that symmetries broken in the mean-field formulation are respected in the RPA treatment so that spurious states lie at zero excitation energy. The classic example of this is the spurious $1^-T=0$ level arising because the usual mean-field treatment is not manifestly covariant. The covariance of the nucleon-nucleon interaction and the MFT RPA consistency guarantee a $1^-T=0$ spurious state at $\omega=0$ which carries all of the lowest order $E1$ strength. Such a state is the RPA approximation to the degenerate translated ground state.

In addition to these features, the fact that the transition currents are conserved at the mean-field level combined with the structure of the RPA equation results in an exactly conserved RPA transition current. All of the properties of the RPA discussed above are realized in the numerical results to be presented here.

IV. SPECTRAL RPA

We now examine two distinct techniques for solving the integral equation which results from combining the MFT version of Eq. (3.8) with Eq. (3.16). The first makes use of a spectral expansion of the MFT propagator [Eq. (2.5)]. This yields

$$-\Pi^{ij;kl}_{\mathrm{MF}}(\mathbf{x},\mathbf{y};\omega)=\sum_{\substack{F\geq\beta\geq 0\\ \alpha}}\left[\frac{\psi^i_\alpha(\mathbf{x})\bar{\psi}^j_\beta(\mathbf{x})\psi^k_\beta(\mathbf{y})\bar{\psi}^l_\alpha(\mathbf{y})}{\omega-\omega_{\alpha\beta}+\iota\eta_\alpha}-\frac{\psi^i_\beta(\mathbf{x})\bar{\psi}^j_\alpha(\mathbf{x})\psi^k_\alpha(\mathbf{y})\bar{\psi}^l_\beta(\mathbf{y})}{\omega+\omega_{\alpha\beta}-\iota\eta_\alpha}\right] \tag{4.1}$$

where $\eta_\alpha=+(-)\eta$ for $\alpha>(\leq)F$ and $\omega_{\alpha\beta}\equiv\epsilon_\alpha-\epsilon_\beta$. The similarity of the Lehmann representation of the full Π [Eq. (3.2)] and the spectral form of Π_{MF} motivates us to define the *particle-hole* transition densities:

$$\mathcal{F}^{kl}_{\alpha\beta}(\mathbf{y})\equiv\psi^k_\beta(\mathbf{y})\bar{\psi}^l_\alpha(\mathbf{y}) \tag{4.2}$$

in analogy with the full $\mathcal{F}^{(n)}$ of Eq. (3.4). This allows us to rewrite Eq. (4.1) in matrix form as

$$-\Pi^{ij;kl}_{\mathrm{MF}}(\mathbf{x},\mathbf{y};\omega)=\sum_{\substack{F\geq\beta\geq 0\\ \alpha}}(\bar{\mathcal{F}}^{ij}_{\alpha\beta}(\mathbf{x}),\bar{\mathcal{F}}^{ij}_{\beta\alpha}(\mathbf{x}))\begin{bmatrix}G_{\alpha\beta}(\omega+\iota\eta_\alpha) & 0\\ 0 & -G^*_{\beta\alpha}(\omega^*+\iota\eta_\alpha)\end{bmatrix}\begin{bmatrix}\mathcal{F}^{kl}_{\alpha\beta}(\mathbf{y})\\ \mathcal{F}^{kl}_{\beta\alpha}(\mathbf{y})\end{bmatrix} \tag{4.3}$$

where we have defined

$$G_{\alpha\beta}(\omega)\equiv\frac{1}{\omega-\omega_{\alpha\beta}}\ .$$

We now assume that the RPA transition density for the excitation of the nth state can be written as

$$\mathcal{F}^{(n)}_{\mathrm{RPA}}=\sum_{\substack{F\geq\beta\geq 0\\ \alpha}}\begin{bmatrix}X^{(n)}_{\alpha\beta}\mathcal{F}_{\alpha\beta}\\ Y^{(n)}_{\alpha\beta}\mathcal{F}_{\beta\alpha}\end{bmatrix} \tag{4.4}$$

where we have dropped the Dirac indices. The RPA integral equation [Eq. (3.8)] can then be recast into the familiar spectral RPA matrix relations:

$$\begin{aligned}&(\omega_n-\omega_{\alpha\beta})X^{(n)}_{\alpha\beta}-\sum_{\substack{F\geq\beta'\geq 0\\ \alpha'}}[K_{\alpha\beta;\alpha'\beta'}(\omega_n)X^{(n)}_{\alpha'\beta'}+K_{\alpha\beta;\beta'\alpha'}(\omega_n)Y^{(n)}_{\alpha'\beta'}]=0\ ,\\ &(\omega_n+\omega_{\alpha\beta})Y^{(n)}_{\alpha\beta}+\sum_{\substack{F\geq\beta'\geq 0\\ \alpha'}}[K_{\beta\alpha;\alpha'\beta'}(\omega_n)X^{(n)}_{\alpha'\beta'}+K_{\beta\alpha;\beta'\alpha'}(\omega_n)Y^{(n)}_{\alpha'\beta'}]=0\end{aligned} \tag{4.5}$$

where

$$K_{\alpha\beta;\alpha'\beta'}(\omega_n)\equiv\sum_{\substack{mm'\\nn'}}\int d^3x_1 d^3x_2\,\mathcal{J}^{mm'}_{\alpha\beta}(\mathbf{x}_1)\left[\sum_{N,ab}(\Gamma^a_N)^{m'm}D_{N;ab}(\mathbf{x}_1-\mathbf{x}_2;\omega_n)(\Gamma^b_N)^{n'n}\right](\bar{\mathcal{J}}_{\alpha'\beta'})^{nn'}(\mathbf{x}_2) \tag{4.6}$$

is the RPA kernel whose ω dependence is typically ignored. This amounts to dropping "retardation effects."

An important property of the RPA presented here can be derived (see Appendix A) using the RPA matrix equations. We observe that the uncorrelated MFT electromagnetic particle-hole transition current is conserved in the following sense. Define the particle-hole transition current via

$$J^\mu_{\alpha\beta}\equiv\int d^3r\, e^{-\iota\mathbf{q}\cdot\mathbf{r}}\mathrm{Tr}[J^\mu\mathcal{J}_{\alpha\beta}(\mathbf{r})] \tag{4.7}$$

where $\mathbf{q}$ is the three-momentum transfer of the transition and where, omitting form factors and isospin labels,

$$J^\mu=-\iota\left[e\gamma^\mu+\frac{\iota\kappa}{2m}\sigma^{\mu\nu}q_\nu\right]$$

is the free nucleon current operator. Since the anomalous moment contribution is divergenceless by construction, we can let $J^\mu\rightarrow-\iota e\gamma^\mu$ for the present discussion of current conservation. Because the single particle wave functions which appear in $\mathcal{J}_{\alpha\beta}$ both satisfy the same Dirac equation [Eq. (2.4)], we have

$$q\cdot J_{\alpha\beta}=0$$

for $q^\mu\equiv(\omega_{\alpha\beta},\mathbf{q})$. The RPA transition current is

$$J^{(n)}_\mu=\int d^3r\, e^{-\iota\mathbf{q}\cdot\mathbf{r}}\mathrm{Tr}[J_\mu\mathcal{J}^{(n)}_{\mathrm{RPA}}(\mathbf{r})] \tag{4.8}$$

and, by the RPA equations [Eq. (4.5)], satisfies

$$q\cdot J^{(n)}=0$$

for $q^\mu\equiv(\omega_n,\mathbf{q})$. Thus, in the present model, the electromagnetic RPA transition current is exactly conserved, ensuring that, among other things, Seigert's theorem is automatically satisfied.

The spectral QHD1-MFT RPA equations have been solved by Furnstahl,[7] by Furnstahl and Dawson,[8,9] and by Blunden and McCorquodale[10] at various levels of approximation. For example, in Refs. 7 and 10, contributions from the negative energy sea [i.e., from $\alpha<0$ in Eq. (4.5)] were ignored. In all cases, the continuum (or *continua* in the case of Refs. 8 and 9 where negative-energy contributions were included) was discretized by "putting the system in a box." This treatment has little effect on the properties of discrete excited states but gives an incorrect picture of the nuclear response in the continuum. Finally, as a necessary consequence of using the spectral method, the discretized Hartree basis is truncated. In Refs. 7 and 10 only positive-energy levels with kinetic energies below $\approx$40 MeV were retained. In Refs. 8 and 9, a much larger basis was used, including positive-energy levels up to several hundred MeV as well as all bound negative-energy states. Altogether, a total of about 200 basis states was employed. Specific results of the large basis calculations of Refs. 8 and 9 will be discussed in Sec. VI where our calculations for discrete transitions are presented.

V. NONSPECTRAL RPA

An alternative to the "spectral" formulation is the direct solution of the MFT version of the RPA integral equation, Eq. (3.8). This "nonspectral" approach is implemented by computing Π_{MF} as given in Eq. (3.16) using the nonspectral MFT propagator G_{MF} as given in Eq. (2.6). Beginning with this form of G_{MF}, a partial-wave version of the RPA integral equation (see Appendix B) may be solved numerically. Specifically, this radial equation is

$$\begin{aligned}-\iota\Pi^{ij;kl}_{LL'SS'J}(x,y;\omega)=&-\iota\Pi^{ij;kl}_{\mathrm{MF};LL'SS'J}(x,y;\omega)\\&+2\sum_{L'';N,a}\sum_{\substack{mm'\\nn'}}\int_0^\infty z_1^2dz_1\int_0^\infty z_2^2dz_2\,(-\iota)\Pi^{ij;mm'}_{\mathrm{MF};LL''SS_aJ}(x,z_1;\omega)(-\iota g_N)^2(\Gamma^a_N)^{m'm}_D\\&\times\iota f^{(N)}_{L''}(z_1,z_2;\omega)(\Gamma_{N;a})^{n'n}_D(-\iota)\Pi^{nn';kl}_{L''L'S_aS'J}(z_2,y;\omega)\end{aligned} \tag{5.1}$$

where $\Pi^{ij;kl}_{\mathrm{MF};LL'SS'J}(x,y;\omega)$ comes from the partial-wave decomposition of Π_{MF} [Eq. (3.16)] and $f^{(N)}_{L''}(z_1,z_2;\omega)$ comes from the Slater expansion of the free meson propagator for meson N. The Dirac matrix content of the meson-nucleon-nucleon vertex for meson type N, namely $(\Gamma_{N;a})^{m'm}_D$ as well as its Pauli spin nature indicated by S_a, are as defined in Appendix B.

There are several advantages to the "nonspectral" method. For example, discretization is avoided and the correct continuum boundary conditions are automatically included. This provides a more realistic continuum response and is crucial for treating, e.g., the quasielastic response in (e,e') or (p,p'). In addition, the entire MFT single particle spectrum—including positive- and negative-energy continua—is automatically incorporated in the G_{MF} of Eq. (3.8). This means that uncertainties inherent in any basis truncation do not arise. Finally, retardation effects [ω dependence of $D^0_{N;ab}(\mathbf{z}_1-\mathbf{z}_2;\omega)$ in Eq. (3.8)] can be trivially included. (This dependence, however, is expected to be very weak in the direct-only RPA discussed here.)

Typically the numerical solution to Eq. (5.1) is found

either by iteration or by matrix inversion after the integrals are put on a Gauss-Laguerre radial grid (see, e.g., Ref. 14 for a similar nonrelativistic approach). The nonspectral Dirac RPA method has been applied to finite nuclei by Shepard *et al.*,[12] Iichi *et al.*,[15] and Wehrberger and Beck.[11] The first two of these studies were aimed at evaluating RPA-like core-polarization corrections to the isoscalar magnetic response of closed-shell ± 1 nuclei. Here the iterative and matrix-inversion techniques gave essentially identical results. In Ref. 11, the iterative technique was used to find the transverse and longitudinal (e,e') responses in the quasielastic region. In this instance, the iterative technique was found to be unreliable in certain kinematic regions. We have recently developed a code[16] for solution via matrix inversion of Eq. (5.1) as it stands for arbitrary complex ω. The calculation is done in configuration space and yields the general result $\Pi^{ij;kl}_{LL'SS'J}(x,y;\tilde{\omega})$, where $\tilde{\omega}=\omega+\iota\eta$ which ensures the *causal* polarization insertion is evaluated as discussed in Sec. III. The flexibility of the code allows us to extract several interesting quantities. We can find the response to any one-body vertex operator at arbitrary ω by solving for Π and taking the traces over the Dirac indices $ij;kl$ as indicated in Eq. (3.6). Alternatively, for a discrete transition, we can evaluate Π at $\tilde{\omega}=\omega_n+\iota\eta$, extract the residue, and determine the RPA transition density $\mathcal{T}^{(n)}_{\rm RPA}$, analogous to the full transition density defined in Eq. (3.4). (See Appendix C for details of the construction of the nonspectral form of $\mathcal{T}^{(n)}_{\rm RPA}$.) This object can then be used in standard scattering codes[17] for (e,e') and (p,p') reactions to compute observables with RPA transition densities without resorting to the usual representation in terms of particle-hole pairs $(\alpha\beta)$ and associated $X^{(n)}_{\alpha\beta}$ and $Y^{(n)}_{\alpha\beta}$ coefficients [see Eq. (4.4)]. We note that the iterative technique for finding Π fails utterly for discrete transitions.

VI. DISCRETE TRANSITIONS

We begin consideration of specific transitions by discussing $1^-T=0$ transitions in ^{16}O. We find a very collective excitation at $\omega=0.5\iota$ MeV which clearly is the spurious level referred to in Sec. III. A clear indication of the correct treatment of spuriosity in our calculations is the behavior of the (e,e') Coulomb form factor for the first *nonspurious* $1^-T=0$ level. This state is calculated to lie at 8.47 MeV, considerably lower than the lowest uncorrelated excitation at 11.2 MeV. The experimental energy is 7.117 MeV suggesting insufficient collectivity in the calculations.

This suggestion is further supported by the comparison in Fig. 1 of calculated (e,e') Coulomb form factors with the data of Buti *et al.*[18] The RPA form factor lies below the data by a factor of $\simeq 2.5$. Note, however, the dramatic difference in shape between the uncorrelated and RPA results which is a consequence of the elimination of all spurious components in the latter. This means that, at small q, F_C^2 is proportional to q^2 in the uncorrelated case but proportional to q^6 for the RPA. Hence the RPA form factor and the data have the same shape as the $3^-T=0$ form factor to be examined below. Also shown

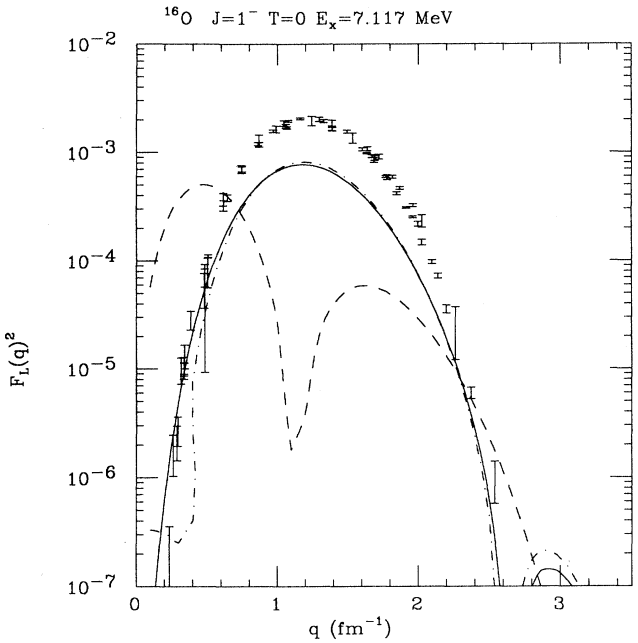

FIG. 1. The Coulomb form factor for the 7.117-MeV $1^-T=0$ level in ^{16}O. The dashed curve is the simple Hartree particle-hole result for a $(p_{1/2})^{-1}(s_{1/2})$ configuration ($E_x=11.2$ MeV) while the solid line is the RPA result ($E_x=8.47$ MeV). The dashed-dotted curve is RPA calculation ($E_x=10.1$ MeV) omitting the correlations due to the spacelike ω interaction. Data are from Ref. 18.

in Fig. 1 is a RPA result which excludes the correlations induced by the spacelike ω interaction. In effect, this calculation employs a noncovariant nucleon-nucleon interaction which means the $1^-T=0$ spuriosity is not treated correctly. The anomalous low-q structure in this form factor is a consequence of less-than-complete elimination of spurious components. The low-q behavior of F_C^2 also determines the $B(E1)$ values of the transition. In Table I various $B(E1)$'s for the lowest $1^-T=0$ level are compared. Two RPA values are given, one deduced from F_C^2 and the other from the transverse electric form factor F_E^2. According to Seigert's theorem or, more generally, current conservation, these two values should be identical. Since both are quenched by RPA correlations by nearly 4 orders of magnitude, their near equality is an indication of sufficient numerical accuracy in our computer program.

As stressed in Sec. III, the RPA discussed here is a consistent extension of the description of the ground state to $1p$-$1h$ excitations of the ground state. This consistency has been emphasized by Frois and Papanicolas[19] in the context of nonrelativistic models. They observe that non-

TABLE I. Calculated $B(E1)$'s for the lowest $1^-T=0$ level in ^{16}O; see text.

Calculation	$B(E1,T=0)e^2\cdot$fm^2
Uncorrelated	8.0×10^{-2}
RPA, Coulomb	1.30×10^{-5}
RPA, Electric	0.93×10^{-5}

relativistic mean-field models predict more structure in the interior region of the ground state charge density than is observed in elastic electron scattering. Similarly, the RPA transition charge densities for the lowest 3^- excitations are more highly structured than the measured quantities. This suggests such a comparison be made using relativistic models, especially since one of the distinctive features of QHD1-MFT calculations[1,2] is a reduction in the interior structure of ground state charge densities relative to nonrelativistic results.

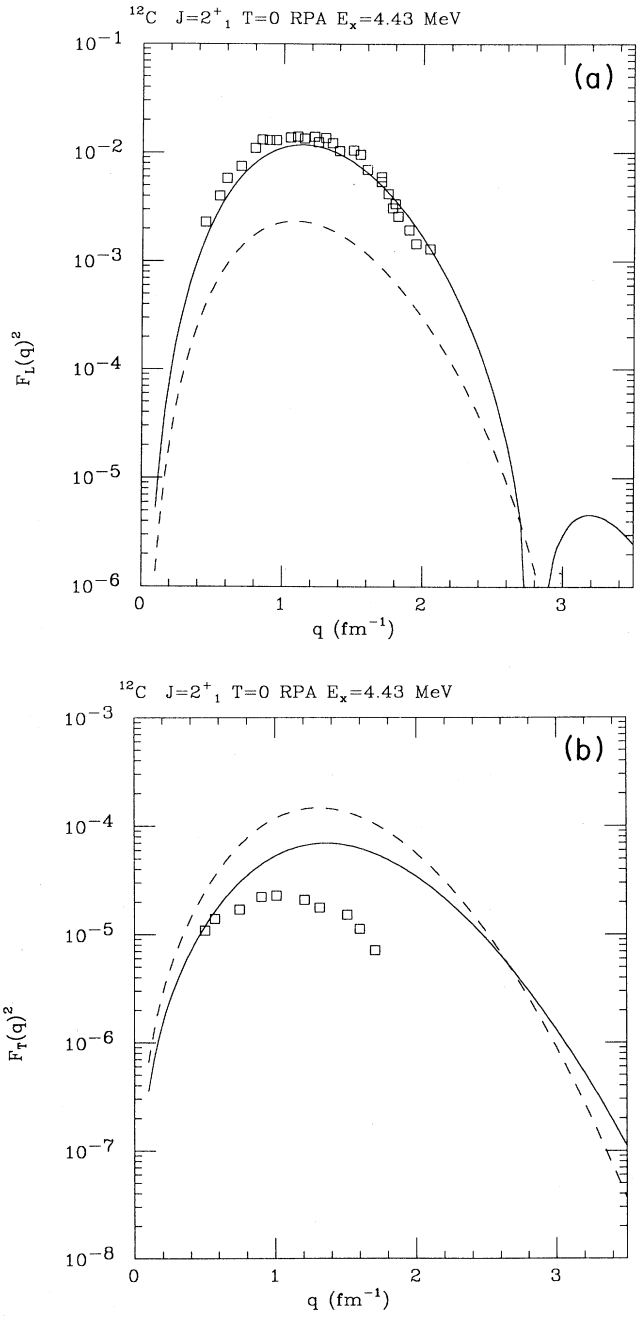

FIG. 2. The Coulomb and transverse electric form factors for the 4.44-MeV $2^+T=0$ level in ^{12}C. The dashed curve is the simple Hartree particle-hole result for a $(p_{3/2})^{-1}(p_{1/2})$ configuration ($E_x=10.92$ MeV) while the solid line is the RPA result ($E_x=4.09$ MeV). Data are from Ref. 20.

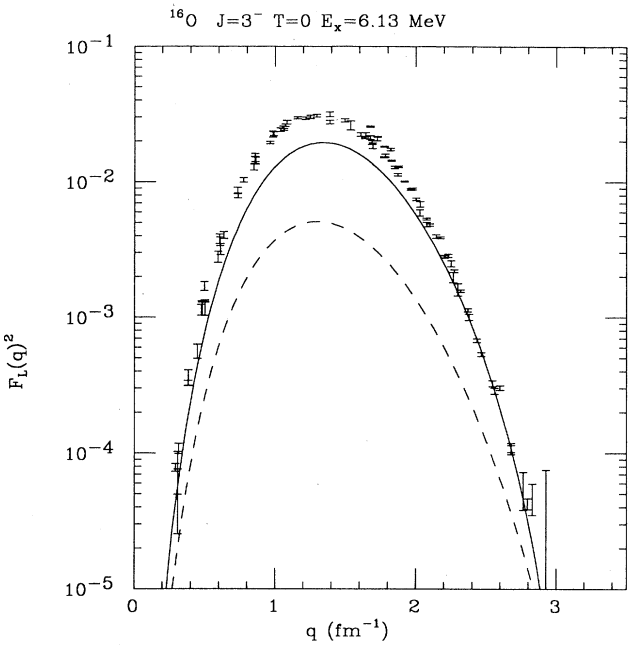

FIG. 3. The Coulomb form factor for the 6.13-MeV $3^-T=0$ level in ^{16}O. The dashed curve is the simple Hartree particle-hole result for a $(p_{1/2})^{-1}(d_{5/2})$ configuration ($E_x=9.11$ MeV) while the solid line is the RPA result ($E_x=5.99$ MeV). Data are from Ref. 18. The normalization of $F_L(q)^2$ differs by a factor of $Z^2/4\pi$ from the other figures.

Our RPA (e,e') Coulomb form factor for the first $2^+T=0$ level in ^{12}C is compared with data in Fig. 2. The RPA correlations enhance the square of the form factor

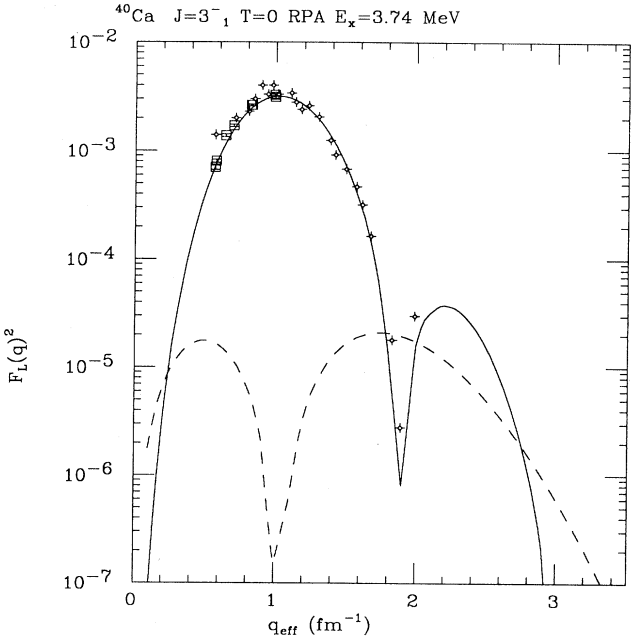

FIG. 4. The Coulomb form factor for the 3.74-MeV $3^-T=0$ level in ^{40}Ca. The dashed curve is the simple Hartree particle-hole result ($E_x=6.39$ MeV) while the solid line is the RPA result ($E_x=2.97$ MeV). Data are from Ref. 25.

at the peak by a factor of 5 and drop the excitation energy from the uncorrelated value of 10.92 MeV to 4.09 MeV. The experimental value is 4.43 MeV. Overall the calculations are in good agreement with data. The transverse electric form factor is also compared with measurements in Fig. 2. We observe that, here, the RPA correlations *quench* the square of the form factor at the peak by nearly a factor of 2. However, the correlations give rise to enhancement beyond $q = 2.5$ fm^{-1}. This reflects the "frontflow" phenomenon due to spacelike ω correlations and previously observed in the elastic $M1$ form factors of ground states of closed-shell ± 1 nuclei calculated in QHD1 MFT.[12,21] The frontflow is an artifact of dropping vacuum polarization effects and is likely to disappear when vacuum dynamics is treated explicitly.[22] In any case, the square of the transverse form factor is overpredicted at the peak where frontflow is negligible by nearly a factor of 3. This discrepancy is due in part to the strong m^* enhancement of the isoscalar Dirac current characteristic of QHD1 mean-field models.[23] The larger m^* which arises in RHA models[2] should reduce this discrepancy as will a more realistic description of the mean-field ground state[24] which is unlike the spherically symmetric $p_{3/2}$ closed shell assumed here.

Coulomb (e,e') form factors for the lowest 3^- excitations in ^{16}O and ^{40}Ca are compared with data in Figs. 3 and 4, respectively. Agreement with experiment is again quite good. However, the ^{40}Ca case is somewhat problematic since, using the standard finite-nucleus QHD1-MFT coupling constants and meson masses,[2] the energy of the 3^- state is imaginary, indicating the spherical mean-field ground state is unstable. The calculation shown employs a σNN coupling constant arbitrarily reduced by one percent. The significance of this failure of the mean-field model is still an open question.

In Fig. 5, the calculated transition charge density (in configuration space) for the lowest 3^- level in ^{48}Ca is compared with the nonrelativistic calculations and the data of Ref. 26. The relativistic RPA calculations again use the reduced σNN coupling constant and agree much more closely with experiment than the nonrelativistic

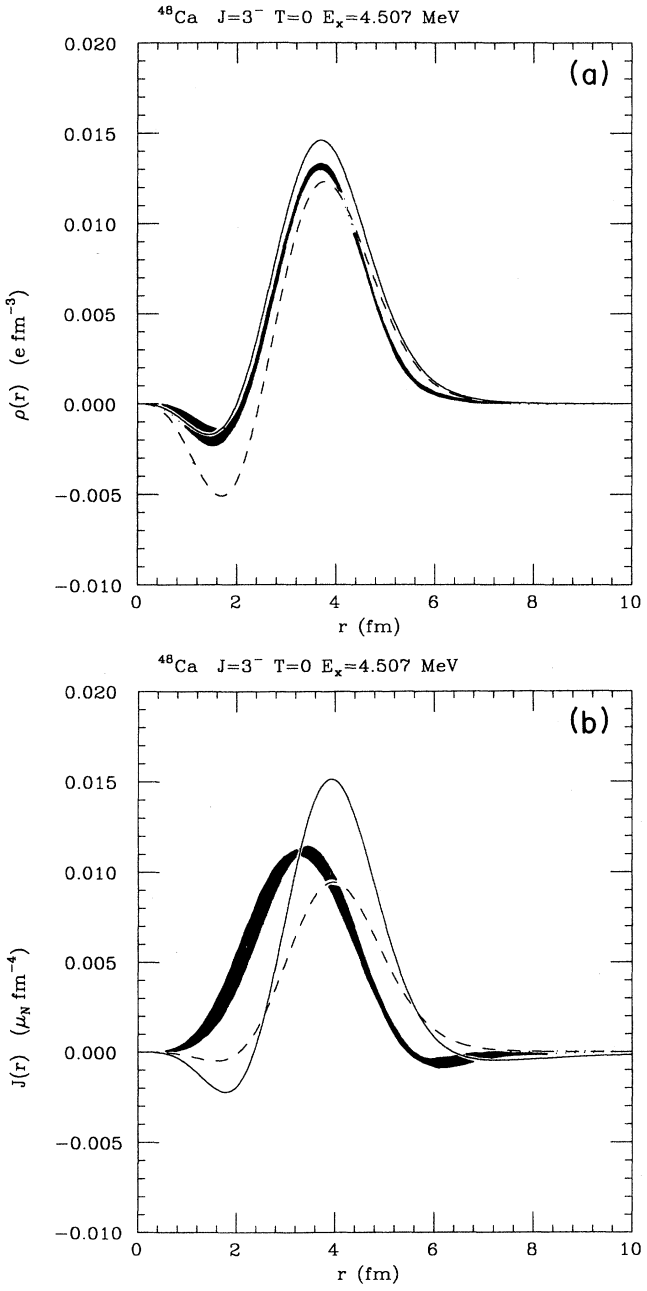

FIG. 5. The charge and current transition densities for the 4.507 MeV 3^- level in ^{48}Ca. The solid curves are the Dirac RPA ($E_x = 4.41$ MeV) results while the dashed lines are the nonrelativistic RPA calculations ($E_x = 4.51$ MeV) of Ref. 26. The experimental values shown by the dark bands are also from Ref. 26.

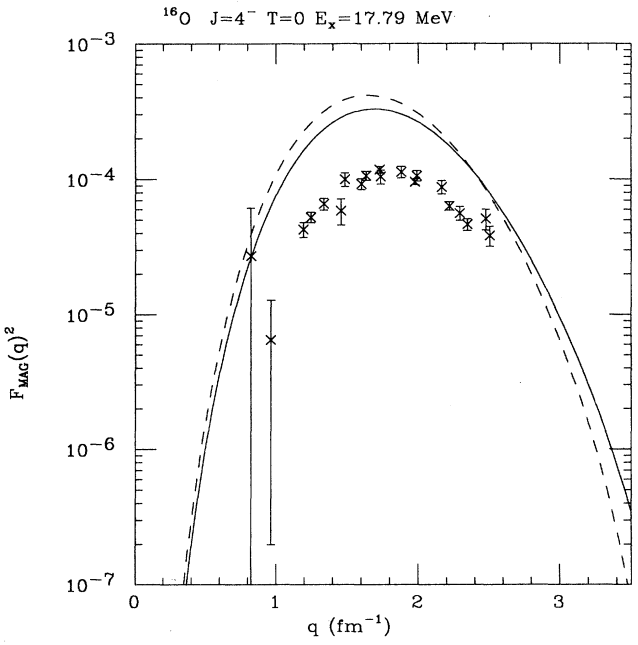

FIG. 6. The magnetic form factor for the 17.79-MeV $4^- T=0$ level in ^{16}O. The dashed curve is the simple Hartree particle-hole result for a $(p_{3/2})^{-1}(d_{5/2})$ configuration ($E_x = 17.37$ MeV) while the solid line is the RPA result ($E_x = 16.225$ MeV). Data are from Ref. 27.

prediction even though the input for the latter was adjusted to reproduce properties of this excitation. This comparison suggests that the superior description of ground state charge densities afforded by the relativistic approach does indeed carry over to the transition densities for collective excitations. Comparisons with the transition *current* densities in Fig. 5, however, are not so felicitous. The shape is badly described by both RPA calculations where m^* and frontflow effects cause the relativistic results to overestimate the data considerably. It will be interesting to examine vacuum polarization effects in this specific case as well.

Figure 6 shows calculated magnetic (e,e') form factors for the 17.79-MeV $4^-T=0$ level in ^{16}O along with the data of Ref. 27. Here the frontflow is evident as a high-q enhancement of the RPA result over the uncorrelated calculation. Both calculations overestimate the data by a factor of 3 or 4. Such overestimates are not surprising since isoscalar magnetic transitions are known[27,28] to be strongly quenched by mechanisms whose description lies beyond the scope of the simple RPA employed here. However, vacuum polarization contributions can be expected to reduce this discrepancy somewhat.

VII. SUM RULES IN DIRAC RPA

It is straightforward to derive sum rules for simple particle-hole (i.e., MFT) matrix elements of one-body vertex operators. These sum rules depend on the completeness of the particle-hole basis. In some cases—for example, in the case of the energy-weighted sum rule to be discussed below—these sum rules are preserved in the RPA (see, e.g., Refs. 4 and 5). In this section, we will consider energy-weighted sums in the (uncorrelated) MFT and then examine numerically the influence of RPA correlation on these quantities. In a *nonrelativistic* picture, the energy-weighted summed response is, using Eq. (3.7),

$$S_{\mathcal{O}} \equiv \int_0^\infty d\omega\, \omega S_{\mathcal{O}}(\omega) = \sum_{\substack{\beta \le F \\ \alpha}} \omega_{\alpha\beta} |\langle \mathcal{O} \rangle_{\alpha\beta}|^2 \tag{7.1}$$

where the hole index β runs over all occupied orbitals. The α index is originally taken to run over all unoccupied states but, because of the antisymmetry of $\omega_{\alpha\beta}$ under interchange of indices, the range of α can be extended to include the range of β. Thus in this expression the range of α is unrestricted. Still, the only nonvanishing contributions to $S_{\mathcal{O}}$ arise from terms with $\alpha > F$ which ensures $\omega_{\alpha\beta}$ is positive and that $S_{\mathcal{O}}$ is positive definite. Assuming, in analogy with Eq. (2.4), that the single particle wave functions are eigenfunctions of a single particle Hamiltonian,

$$h|\alpha\rangle = \epsilon_\alpha |\alpha\rangle$$

we can show

$$S_{\mathcal{O}} = \tfrac{1}{2} \sum_{\beta \le F} \langle \beta | [\mathcal{O}, [h, \mathcal{O}]] | \beta \rangle \tag{7.2}$$

where we have made use of the completeness relation

$$\sum_\alpha |\alpha\rangle\langle\alpha| = 1 \ . \tag{7.3}$$

In the QHD1-MFT RPA presented here, the analogue to Eqs. (7.1) and (7.2) is (remembering to construct the response from the retarded polarization insertion $\Pi_{\text{MF:ret}}$)

$$S_{\mathcal{O}} = \sum_{\substack{F \ge \beta > 0 \\ \alpha}} \omega_{\alpha\beta} |\langle \mathcal{O} \rangle_{\alpha\beta}|^2 = \tfrac{1}{2} \sum_{F \ge \beta > 0} \langle \beta | [\mathcal{O}, [h, \mathcal{O}]] | \beta \rangle \tag{7.4}$$

where now the hole label β is restricted to positive-energy occupied levels and the particle label α runs over the entire Hartree spectrum, including the negative-energy levels. When α refers to a negative-energy level, the corresponding term in the energy-weighted sum rule [Eq. (7.4)] is *negative* definite since $\omega_{\alpha\beta} = \epsilon_\alpha - \epsilon_\beta < 0$. Thus the sum rule strength is no longer positive definite (see Fig. 7).

An example which illustrates the significance of these differences between Dirac MFT and nonrelativistic sum rules is the photoabsorption sum rule. The relevant one-body vertex operator is the electric-dipole operator:

$$\mathcal{O} \to \frac{-ie}{2}(1+\tau_z)\mathbf{r}\cdot\hat{z} \ . \tag{7.5}$$

(This expression is valid both relativistically and nonrelativistically assuming the operator is to be evaluated between single particle wave functions and their Hermitian conjugates, and not, in the relativistic case, between the wave functions and their adjoints.) Nonrelativistically, assuming the potentials in h to be local and independent of isospin, we have

$$[\mathcal{O}, [h, \mathcal{O}]] = \tfrac{1}{2}(1+\tau_z)\frac{1}{m} \tag{7.6}$$

which yields the (non-recoil-corrected) TRK sum rule

$$\sigma_0 = \frac{2\pi^2\alpha}{m}\frac{NZ}{A} \ . \tag{7.7}$$

Relativistically, as pointed out by Price and Walker,[29]

$$[\mathcal{O}, [h, \mathcal{O}]] = 0$$

and the summed photoabsorption strength vanishes. What is the physical interpretation of this result? We consider the MFT version of the (spectral) response to a probe with interaction vertex $\mathcal{O}$. In analogy with Eq. (3.7), this quantity is

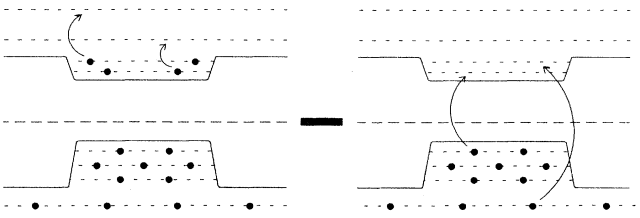

FIG. 7. Schematic representation of nuclear response contained in mean-field-theory polarization insertion. See text.

$$S_{\mathcal{O}}^{\mathrm{MF}}(\omega)=\sum_{\substack{F\geq\beta>0\\ \alpha}}|\langle\mathcal{O}\rangle_{\alpha\beta}|^2[\delta(\omega-\omega_{\alpha\beta})-\delta(\omega+\omega_{\alpha\beta})]\ , \tag{7.8}$$

where $\langle\mathcal{O}\rangle_{\alpha\beta}\equiv\mathrm{Tr}(\mathcal{O}\mathcal{T}_{\alpha\beta})$ and where $\mathcal{T}_{\alpha\beta}$ is the particle-hole transition density defined in Eq. (4.2). For *positive* ω, the first term of Eq. (7.8) contributes only for $\alpha>F$. This is the Dirac analogue to the usual "particle-hole" response in the nonrelativistic RPA. A unique feature of the Dirac RPA is that the second δ function—which usually can be nonzero only for *negative* ω and is thus associated with the decay of excited states—*can* contribute for ω positive since $\omega_{\alpha\beta}=\epsilon_\alpha-\epsilon_\beta<0$ for $\epsilon_\alpha<0$. These contributions describe the *blocking* of the response of vacuum due to the presence of occupied, positive-energy states, ψ_β. We immediately see that the energy-weighted sum is

$$S_{\mathcal{O}}^{\mathrm{MF}}=\sum_{\substack{F\geq\beta>0\\ \alpha}}\omega_{\alpha\beta}|\langle\mathcal{O}\rangle_{\alpha\beta}|^2\ . \tag{7.9}$$

In contrast to the nonrelativistic case [Eq. (7.1)] where all terms in the sum were positive definite, $\omega_{\alpha\beta}<0$ for $\epsilon_\alpha<0$ and these terms are negative definite. Thus, when the double commutator of $\mathcal{O}$ with the MFT Hamiltonian vanishes, as is the case for the electric-dipole operator, we understand that the ordinary particle-hole ($\alpha>F$) contribution is exactly canceled by the blocking response ($\alpha<0$). This accounts for the zero photoabsorption sum rule in our model. As pointed out in Ref. 29, the negative contributions to the sum rule involve $\alpha<0$ and thus correspond to pair creation and so to very high "excitation" energies. By restricting the range of energy integration in the sum rule [Eq. (7.1)] to exclude such pair processes, these negative contributions are dropped and, instead of a summation over all particle states α, only positive energy α are included. Then, using

$$\sum_{\alpha>0}|\alpha\rangle\langle\alpha|=\Lambda^{(+)} \tag{7.10}$$

where $\Lambda^{(+)}$ is the positive-energy projection operator, the "projector" sum rule becomes

$$S_{\mathcal{O}}^{(+)}=\tfrac{1}{2}\sum_{F\geq\beta>0}\langle\beta|(\mathcal{O}\Lambda^{(+)}[h,\mathcal{O}]-[h,\mathcal{O}]\Lambda^{(+)}\mathcal{O})|\beta\rangle \tag{7.11}$$

and the nonrelativistic sum rule [Eq. (7.7)] is (approximately) recovered.[29] In our calculations, the completeness properties of a finite basis-spline approach to the spectral RPA (Ref. 30) are exploited to represent efficiently the positive-energy projection operator.

In the RPA, contributions from the ordinary particle-hole excitations are mixed with pair contributions and only the *full* sum rule of Eq. (7.2) is preserved. Thus, in the finite-basis spectral RPA calculations,[30] only the trivial, zero photoabsorption sum rule is rigorously satisfied. Any "sum rule" for excitations below $N\bar{N}$ threshold will be approximate and model dependent.

In order to examine the extent to which the effective "no-pair" QHD1-MFT RPA rules differ from the nonrelativistic and "projector" sum rules, we have directly evaluated the energy-weighted sum for the isoscalar (e,e') Coulomb quadrupole response in ^{40}Ca. The MFT and RPA responses at $q=200$ MeV/c are displayed in Fig. 8. The energy-weighted sums obtained from these responses are compared with the nonrelativistic [i.e., Eq. (7.2) with $h\rightarrow-\nabla^2/2m$] and projector [i.e., Eq. (7.11)] sum rules at several values of three-momentum transfer in Table II. The comparison reveals that, for this particular response, the projector sum rule is enhanced over the nonrelativistic one by 20–30%, presumably due to m^* enhancements of currents. Also shown in Table II is the summed mean-field response obtained by direct integration of the uncorrelated (e,e') spectrum up to 100 MeV. For $q\leq150$ MeV/c, this summed response agrees well with the projector sum rule suggesting that the assumptions discussed above Eq. (7.10) are well satisfied. For higher q's, excitation energies above 100 MeV become increasingly important and the summed response lies below the full projected sum rule because of the arbitrarily restricted range of integration over ω.

As noted above, ordinary $1p$-$1h$ excitations mix with pair-production terms in the RPA and only the full sum rule of Eq. (7.4) is preserved. However, Table II shows that the summed QHD1-MFT RPA response, again obtained by direct integration of the spectrum, is nearly identical to the projector sum rule at low q. For $q\geq200$ MeV/c, RPA correlations reduce the energy-weighted sum by as much as 25% presumably due to a shift of strength above the 100 MeV upper limit of our integration.

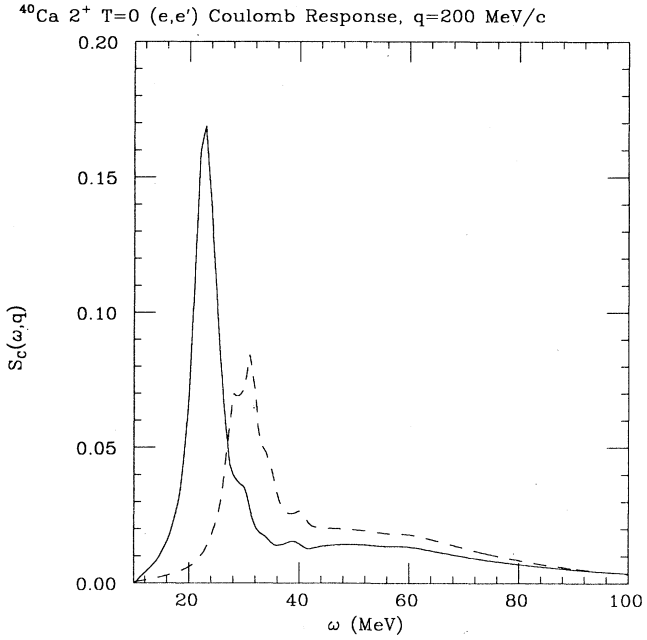

FIG. 8. The ^{40}Ca isocalar (e,e') Coulomb quadrupole responses in MFT (dashed line) and MFT RPA (solid line) are shown. In these calculations, the nucleon electromagnetic form factor was set to unity, retardation effects and spacelike ω correlations were omitted, and the response was folded with a Breit-Wigner having a half-width of 1.5 MeV.

TABLE II. Energy-weighted sum of (e,e') isoscalar quadrupole Coulomb response for ^{40}Ca; see text.

q (MeV/c)	S^{NR} (MeV)	$S^{(+)}$	S^{MFT}		S^{RPA}	
			$\%S^{NR}$	$\%S^{NR}$	$\%S^{(+)}$	$\%S^{NR}$	$\%S^{(+)}$
50	1.74	2.18	125%	126%	101%	129%	103%
150	38.45	51.15	133%	135%	102%	135%	102%
200	57.06	75.56	132%	127%	96%	120%	91%
250	72.71	94.00	129%	102%	79%	85%	66%
400	91.10	112.36	123%	21%	17%	16%	13%

The awkwardness of the sum rules in this version of the QHD1-MFT RPA is related to the fact that we have omitted vacuum polarization contributions to the nuclear response. While the significance of the QHD vacuum is quite controversial at present, inclusion of vacuum polarization terms in future formulations will at least give more physically meaningful sum rules. For example, renormalization will permit the calculation of the difference between the response of the nucleus and the response of the *true* isotropic vacuum. This difference is an observable quantity.

VIII. GIANT RESONANCES

In Sec. VI, we outlined the treatment of discrete excitations in our nonspectral RPA. This approach exploits the relationship appearing in Eq. (3.3) which states that, for ω sufficiently close to ω_n, the excitation energy of the nth state, a single pole dominates Π and the residue at this pole is the "outer product" of the transition density $\mathcal{J}$ and its adjoint. This picture can be straightforwardly extended to account for giant resonances. This extension is most readily understood by considering the spectral form of the uncorrelated polarization insertion, Π_{MF}, given in Eq. (4.1). It is evident that this object has poles at $\omega_{\alpha\beta}$, the particle-hole excitation energies. We recall $\omega_{\alpha\beta}\equiv\epsilon_\alpha-\epsilon_\beta$ where the ϵ's are the single particle energies for the MFT Dirac equation. Since the hole index β refers to a level below the Fermi surface, this level must be bound and ϵ_β must be real. If the particle index α also corresponds to a bound single particle level, ϵ_α is also real, Π_{MF} has a pole at $\omega_{\alpha\beta}$ *on the real axis,* and the methods of Sec. VI apply directly.

Now consider the case for which the particle index α refers to a *resonant* single particle level. As is well known, such levels have complex "eigenenergies," $\epsilon_\alpha\rightarrow\epsilon_\alpha-\iota\Gamma_\alpha/2$ where Γ_α is the escape width of the resonance. (In fact, it is more precise to say that resonant states correspond to poles in the single particle propagator G_{MF} at complex frequencies.[31]) In this instance, the pole in Π_{MF} will appear at the *complex* energy $\omega_{\alpha\beta}=(\epsilon_\alpha-\iota\Gamma_\alpha/2)-\epsilon_\beta$. The contribution of this pole to the continuum response for a probe with a vertex given by the operator $\mathcal{O}$ is, via Eqs. (3.3), (3.5), and (3.7),

$$S_{\mathcal{O}}\rightarrow|\langle\mathcal{O}\rangle_{\alpha\beta}|^2\left[-\frac{1}{\pi}\right]\mathrm{Im}\frac{1}{\omega-(\epsilon_\alpha-\iota\Gamma_\alpha/2-\epsilon_\beta)}$$
$$=|\langle\mathcal{O}\rangle_{\alpha\beta}|^2\frac{\Gamma_\alpha/2\pi}{[\omega-(\epsilon_\alpha-\epsilon_\beta)]^2+(\Gamma_\alpha/2)^2} \quad (8.1)$$

where, in analogy with Eq. (3.5),

$$\langle\mathcal{O}\rangle_{\alpha\beta}\equiv\int d^3y\ \mathrm{Tr}[\mathcal{O}(\mathbf{y})\mathcal{J}_{\alpha\beta}(\mathbf{y})] \quad (8.2)$$

and where $\mathcal{J}_{\alpha\beta}$ is the particle-hole transition density defined in Eq. (4.2). This response is just the modulus squared of the particle-hole matrix element times a Breit-Wigner with full width at one-half maximum of Γ_α. The correct limit [Eq. (3.7)] is obtained for $\Gamma_\alpha\rightarrow 0$. The method outlined in Sec. III and discussed in detail in Appendix C for extracting the transition densities by numerically determining the residue of Π at its poles was applied in Sec. VI to the case of real excitation energies (i.e., poles on the real axis) but is equally appropriate for poles at complex energies. In the present work, the existence of such poles in Π_{MF} is ensured by the continuum boundary conditions imposed in constructing the nonspectral single particle propagator G_{MF}. [See Eq. (2.6) and Appendix B.] We conclude that the technique just outlined is likewise appropriate for the RPA; i.e., we may find poles in Π_{RPA} at complex energies, associate the imaginary part of these energies with the escape widths of the excitations, extract the transition densities by numerically determining the residues of Π_{RPA} at the poles, and compute the contributions of these excitations to the response using the appropriate generalization of Eq. (8.1).

Preliminary investigations of the structure of Π_{RPA} in the complex-ω plane suggest the picture outlined above is realized in our calculations. Figure 8 shows the MFT and RPA (e,e') isoscalar quadrupole responses for ^{40}Ca at a momentum transfer of $q=200$ MeV/c. A large structure appears at $\omega\simeq 30$ (21) MeV in the MFT (RPA) response. Poles in the insertions having large residues are found at complex ω's corresponding to the centroids and widths of these peaks. We identify these poles with (pieces of) the isoscalar giant quadrupole resonance.

In the present picture, then, we think of discrete, low-lying collective transitions and giant resonances in much the same way except that the latter correspond to poles at complex rather than real ω's. We are familiar with the fact that RPA correlations lower the excitation energy and build up the strength of low-lying collective excitations. This amounts to altering the position of a pole on the real axis and increasing its residue. The same picture can be applied to the giant resonaces where now RPA correlations will shift the pole *in the complex-ω plane* affecting both its centroid and escape width. Application of these techniques to specific giant resonances and use of extracted transition densities in (e,e'), (p,p'), and (π,π') calculations will be reported in a future publication.[32]

IX. QUASIELASTIC (e,e') COULOMB RESPONSE

While the preceding discussion of giant resonances is useful for the interpretation of distinct structures in the low energy continuum response, it is not applicable everywhere in the continuum. For example, in the region of the quasielastic response, it is unfeasible to decompose the contribution of each of the many relevant partial waves into contributions due to individual poles. Instead, the response is most readily computed by direct use of Eq. (3.6). We have performed such calculations for the quasielastic (e,e') Coulomb response for ^{12}C and ^{40}Ca. In these calculations, we assume (1) that the isoscalar anomalous moment vanishes and (2) that the isovector response is uncorrelated. We use the nucleon electromagnetic form factors of Ref. 33. Figure 9 shows uncorrelated and RPA calculations for the longitudinal quasielastic response of ^{12}C at $q=400$ and 550 MeV/c. Similar comparisons are made for ^{40}Ca in Fig. 10. The RPA

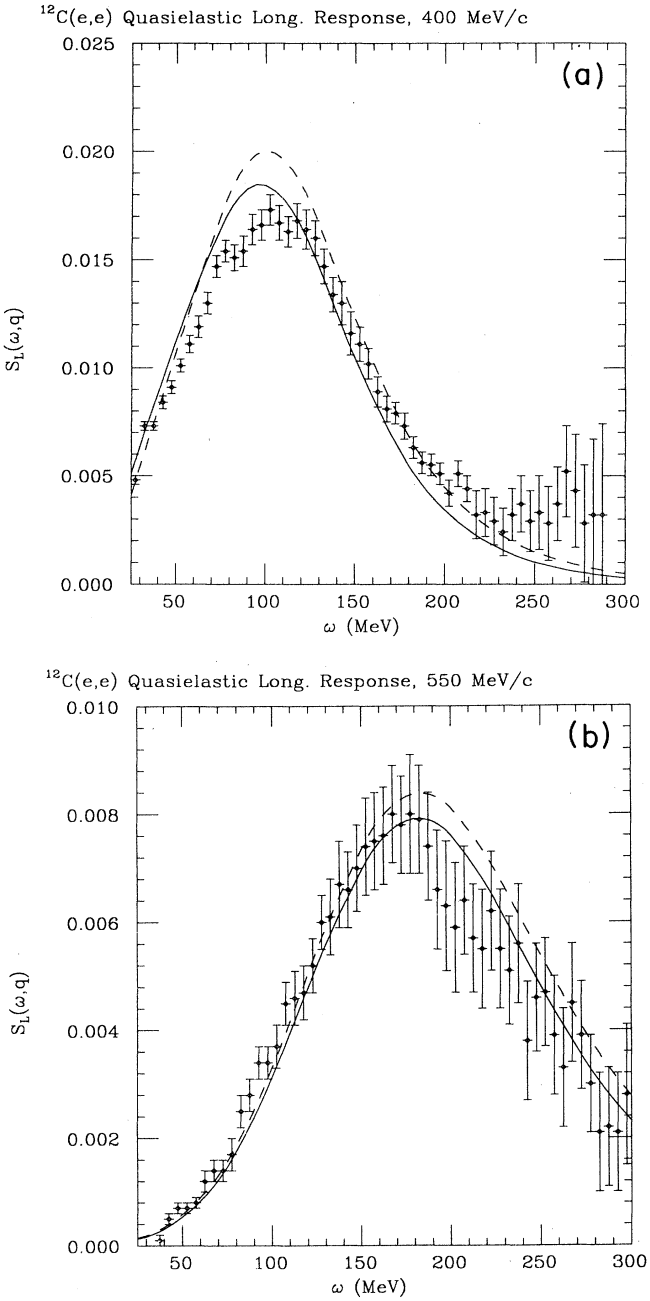

FIG. 9. The longitudinal quasielastic (e,e') response for ^{12}C at $q=400$ and 550 MeV/c is compared with Dirac uncorrelated (dashed) and RPA (solid) calculations. The data are from Ref. 34.

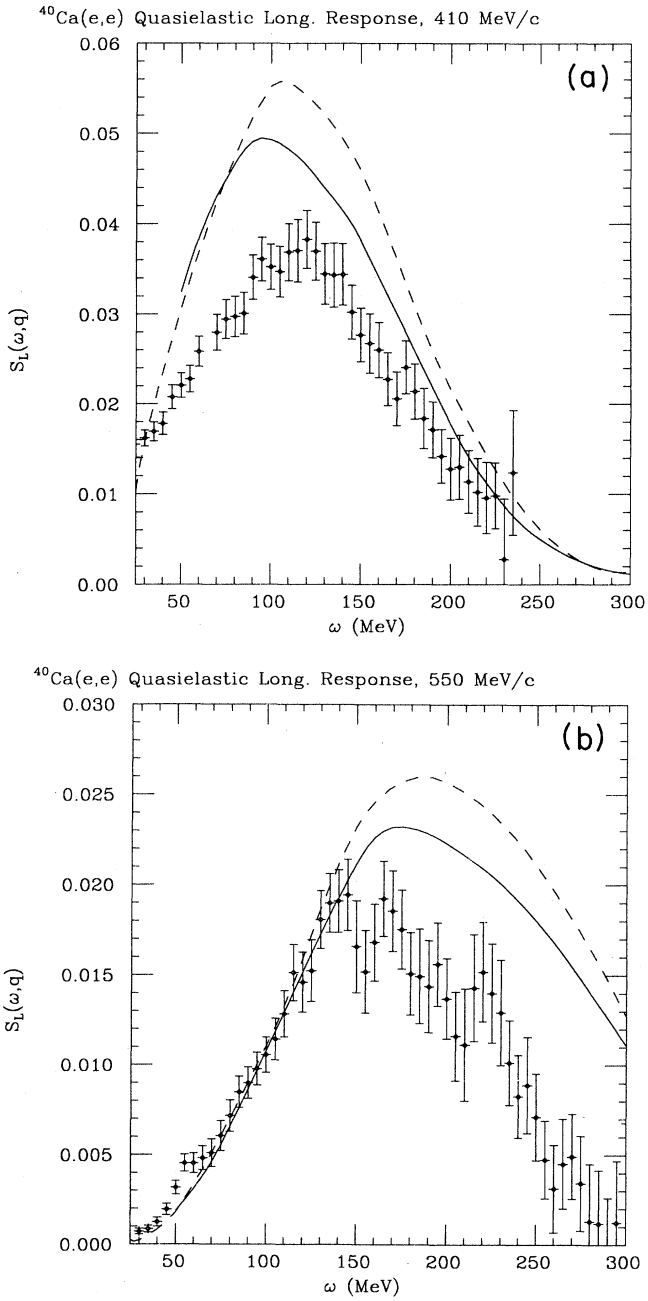

FIG. 10. The longitudinal quasielastic (e,e') response for ^{40}Ca at $q=410$ and 550 MeV/c is compared with Dirac uncorrelated (dashed) and RPA (solid) calculations. The data are from Ref. 34.

response is seen to be appreciably quenched compared to the uncorrelated result and is also in good agreement with the data, especially for ^{12}C. Both Horowitz[35] and Suzuki[36] have observed that this RPA quenching is crucial for describing the experimental Coulomb sum values. Also, as discussed by Horowitz and Piekarewicz,[22,37] vacuum polarization effects somewhat reduce the response on the high-ω side of the quasielastic peak, substantially improving agreement with the ^{40}Ca data but worsening the description of ^{12}C.

X. SUMMARY AND CONCLUSIONS

We have presented Dirac RPA calculations emphasizing their consistency with successful mean-field descriptions of nuclear ground states. We have discussed a calculational approach which avoids the approximations and ambiguities of more conventional RPA treatments by employing a nonspectral single particle propagator. Some Dirac RPA calculations by other workers are discussed in Refs. 7–10. Our method allows consistent treatment of both discrete and continuum excitations including correct boundary conditions in each case. The RPA description of (e,e') Coulomb form factors for low-lying collective excitations is quite good. The associated transverse electric form factors are more poorly reproduced, presumably due to m^* enhancements and "frontflow." Both these phenomena are likely to be substantially reduced by including vacuum polarization contributions.

The energy-weighted summed response in our Dirac RPA was found to be constrained by a sum rule of little physical utility. In the uncorrelated case, it is possible to define a "projected" sum rule which can be closely connected with measurable quantities and which is very similar to the more familiar nonrelativistic sum rule. Numerical examples of various summed responses were presented in the case of the isoscalar quadrupole Coulomb (e,e') response for ^{40}Ca. The projected sum rule was found to be enhanced by 20–30 % over the nonrelativistic result. The Dirac RPA summed response was observed to be very similar to the projected sum rule at low q but somewhat lower at $q \geq 200$ MeV/c.

The correspondence between poles in the polarization insertion at real values of ω and discrete excitations was extended to include giant resonances which appear as poles at complex energies, the imaginary part of which corresponds to the escape width of the resonance. Our method of calculation, which builds in the correct continuum boundary conditions at the level of the nonspectral single particle propagator, naturally gives rise to such poles. We have numerically established the connection between such poles and low-lying peaks of nonzero width in our continuum response. Application to specific resonances, including the use of extracted transition densities to make predictions for (e,e'), (p,p'), and (π,π') observables, will be the subject of future studies.[32]

We have also evaluated quasielastic (e,e') Coulomb responses for ^{12}C and ^{40}Ca. The RPA calculations were found to be in good agreement with data, in most cases correctly reproducing the strong quenching relative to both relativistic Fermi gas and uncorrelated (or mean-field-theory) results.

The model presented here could be improved in several ways. For example, we would like to include explicit treatment of the vacuum dynamics with particular emphasis on their implications for transverse electric form factors. A complete theory of collective excitations must describe both the Coulomb and electric (e,e') form factors. The present RPA is successful only for the former. While examination of electromagnetic observables has been very informative, comparison with (p,p') data is likely to provide interesting and unique tests of the Dirac RPA. To effect such comparisons, we have adapted existing (p,p') codes[17] to accept our nonspectral RPA transition densities. Results of (p,p') calculations employing our RPA transition densities and consistent distortions generated using relativistic impulse approximation optical potentials constructed from experimental NN amplitudes and mean-field-theory vector and scalar ground state densities will be reported elsewhere.[38] Eventually, we hope to calculate the (p,p') continuum response using $\Pi_{\rm RPA}$ and distorted waves determined by the relativistic impulse approximation. It may be possible to treat the distortions in full partial-wave expansion rather than using plane waves or an eikonal formulation. Finally, we must include isovector RPA correlations arising from interactions mediated by π and ρ mesons. Such calculations, using an approach similar to that employed in Ref. 10, are in progress.

ACKNOWLEDGMENTS

The work presented here has benefited from discussions with R. Furnstahl, J. Piekarewicz, C. Horowitz, J. Dawson, C. Price, R. de Haro, R. D. Smith, and R. J. Peterson. We owe particular thanks to R. Furnstahl for an important contribution to the proof of current conservation in the Dirac RPA. This work was supported in part by the U.S. Department of Energy (DOE) and the National Science Foundation (NSF).

APPENDIX A

We first establish that the particle-hole transition current as defined in Eq. (4.7) has zero divergence. Using $q^\mu=(\omega_{\alpha\beta},\mathbf{q})$, we have, letting $e\rightarrow 1$,

$$\begin{aligned} \iota q\cdot J_{\alpha\beta} &\rightarrow \int d^3r\, e^{-\iota \mathbf{q}\cdot\mathbf{r}}\mathrm{Tr}[\not{q}\,\mathcal{F}_{\alpha\beta}(\mathbf{r})] \\ &= \int d^3r\, e^{-\iota \mathbf{q}\cdot\mathbf{r}}\bar{\psi}_\beta(\mathbf{r}) \\ &\quad\times[\gamma^0(\epsilon_\beta-\epsilon_\alpha)-\boldsymbol{\gamma}\cdot\mathbf{q}]\psi_\alpha(\mathbf{r})\ . \end{aligned} \tag{A1}$$

After expressing $\mathbf{q}$ in terms of a gradient acting on the exponential, integration by parts yields

$$\begin{aligned} \iota q\cdot J_{\alpha\beta} &= \int d^3r\, e^{-\iota \mathbf{q}\cdot\mathbf{r}}\bar{\psi}_\beta(\mathbf{r}) \\ &\quad\times[\gamma^0(\epsilon_\alpha-\epsilon_\beta)+\iota\boldsymbol{\gamma}\cdot(\boldsymbol{\nabla}_\beta+\boldsymbol{\nabla}_\alpha)]\psi_\alpha(\mathbf{r}) \end{aligned} \tag{A2}$$

where $\boldsymbol{\nabla}_\alpha$ ($\boldsymbol{\nabla}_\beta$) acts only on ψ_α (ψ_β). Since ψ_α and ψ_β satisfy the same Dirac equation [Eq. (2.4) with MFT self-energies] with eigenvalues ϵ_α and ϵ_β, respectively, the

quantity in the square brackets vanishes and the particle-hole transition current is conserved.

In RPA, the statement of current conservation is

$$q\cdot J_{(n)}=\int d^3r\, e^{-\iota\mathbf{q}\cdot\mathbf{r}}\mathrm{Tr}[\not{q}\mathcal{F}^{(n)}_{\mathrm{RPA}}(\mathbf{r})]=0 \tag{A3}$$

where now $q^\mu=(\omega_n,\mathbf{q})$. To prove this assertion, we use the spectral representation of $\mathcal{F}^{(n)}_{\mathrm{RPA}}$ as given in Eq. (4.4) to write

$$\begin{aligned}\iota q\cdot J_{(n)}&=\sum_{\substack{F\geq\beta>0\\ \alpha}}\Big[X^{(n)}_{\alpha\beta}\int d^3r\, e^{-\iota\mathbf{q}\cdot\mathbf{r}}\mathrm{Tr}[\not{q}\mathcal{F}_{\alpha\beta}(\mathbf{r})]\\ &\qquad+Y^{(n)}_{\alpha\beta}\int d^3r\, e^{-\iota\mathbf{q}\cdot\mathbf{r}}\mathrm{Tr}[\not{q}\mathcal{F}_{\beta\alpha}(\mathbf{r})]\Big]\\ &=\sum_{\substack{F\geq\beta>0\\ \alpha}}[(\omega_n-\omega_{\alpha\beta})X^{(n)}_{\alpha\beta}J^0_{\alpha\beta}\\ &\qquad+(\omega_n+\omega_{\alpha\beta})Y^{(n)}_{\alpha\beta}J^0_{\alpha\beta}]\end{aligned} \tag{A4}$$

where the last expression follows from the conservation of the particle-hole transition current with $q^\mu=(\omega_{\alpha\beta},\mathbf{q})$. The spectral RPA matrix equations [Eq. (4.5)] may now be used to write

$$\begin{aligned}\iota q\cdot J_{(n)}=\sum_{\substack{F\geq\beta,\beta'>0\\ \alpha,\alpha'}}&[J^0_{\alpha\beta}(K_{\alpha\beta;\alpha'\beta'}X^{(n)}_{\alpha'\beta'}+K_{\alpha\beta;\beta'\alpha'}Y^{(n)}_{\alpha'\beta'})\\ &-J^0_{\beta\alpha}(K_{\beta\alpha;\alpha'\beta'}X^{(n)}_{\alpha'\beta'}+K_{\beta\alpha;\beta'\alpha'}Y^{(n)}_{\alpha'\beta'})]\,.\end{aligned} \tag{A5}$$

We now write explicitly,

$$\begin{aligned}J^0_{\alpha\beta}&\rightarrow\int d^3x[\psi_\beta(\mathbf{x})]^{l'}[\psi^\dagger_\alpha(\mathbf{x})]^l[\gamma^0J^0e^{-\iota\mathbf{q}\cdot\mathbf{x}}]^{ll'}\\ &=\int d^3x\, e^{-\iota\mathbf{q}\cdot\mathbf{x}}[\psi^\dagger_\alpha(\mathbf{x})]^l[\psi_\beta(\mathbf{x})]^l\end{aligned} \tag{A6}$$

where l and l' are Dirac spinor indices, a sum over which is implicit, and where we have made use of the explicit form of J^0 (see Sec. IV). Similarly,

$$\begin{aligned}K_{\alpha\beta;\alpha'\beta'}\rightarrow&\int d^3y\, d^3z[\psi_\alpha(\mathbf{y})]^{m'}[\psi^\dagger_\beta(\mathbf{y})]^m\\ &\times[\tilde{K}(\mathbf{y}-\mathbf{z})]^{mm';nn'}[\psi_{\beta'}(\mathbf{z})]^{n'}[\psi^\dagger_{\alpha'}(\mathbf{z})]^n\end{aligned} \tag{A7}$$

where $\tilde{K}$ is the quantity in the large parentheses in Eq. (4.6) but contracted with γ^0 "at each end." The completeness relation is

$$\sum_\alpha[\psi_\alpha(\mathbf{y})]^{m'}[\psi^\dagger_\alpha(\mathbf{x})]^l=\delta_{m',l}\delta^{(3)}(\mathbf{x}-\mathbf{y}) \tag{A8}$$

which implies

$$\begin{aligned}\sum_\alpha J^0_{\alpha\beta}K_{\alpha\beta;\alpha'\beta'}=&\int d^3y\, d^3z\, e^{-\iota\mathbf{q}\cdot\mathbf{y}}[\psi_\beta(\mathbf{y})]^{m'}[\psi^\dagger_\beta(\mathbf{y})]^m\\ &\times[\tilde{K}(\mathbf{y}-\mathbf{z})]^{mm';nn'}[\psi_{\beta'}(\mathbf{z})]^{n'}[\psi^\dagger_{\alpha'}(\mathbf{z})]^n\,.\end{aligned} \tag{A9}$$

Use of the orthogonality relation again in the specific form of

$$\sum_\alpha[\psi_\alpha(\mathbf{x})]^l[\psi^\dagger_\alpha(\mathbf{y})]^m=\delta_{m,l}\delta^{(3)}(\mathbf{x}-\mathbf{y})$$

shows

$$\sum_\alpha J^0_{\beta\alpha}K_{\beta\alpha;\alpha'\beta'}=\sum_\alpha J^0_{\alpha\beta}K_{\alpha\beta;\alpha'\beta'}\,. \tag{A10}$$

Similar results hold when α' and β' are interchanged and $\iota q\cdot J_{(n)}=0$ follows, as required.

The above proof does not depend on any specific properties of the interaction K. In particular, consistency between K and the Hartree basis is *not* necessary for current conservation as it is for proper treatment of spurious excitations (see Sec. III). However, completeness is essential and a conserved RPA current is not obtained with a truncated basis even if the simple particle-hole current is conserved.

APPENDIX B

In this appendix, we derive the partial-wave form of the RPA equation as shown in Eq. (5.1). Using the expression for the MFT polarization insertion, Π_{MF}, given in Eq. (3.16), the first iteration of Π_{MF} is

$$\begin{aligned}-\iota\Pi^{(1)ij;kl}_{\mathrm{MF}}(\mathbf{x},\mathbf{y};\omega)=&\int d^3z_1d^3z_2(-\iota)\Pi^{ij;mm'}_{\mathrm{MF}}(\mathbf{x},\mathbf{z}_1;\omega)\\ &\times\sum_N(\Gamma^a_N)^{m'm}\iota D^0_{N;ab}(\mathbf{z}_1-\mathbf{z}_2;\omega)\\ &\times(\Gamma^b_N)^{n'n}(-\iota)\Pi^{nn';kl}_{\mathrm{MF}}(\mathbf{z}_2,\mathbf{y};\omega)\end{aligned} \tag{B1}$$

where summation over the repeated Dirac component indices is understood. To make further progress, we specify the angular dependence of the quantities comprising Π_{MF}. Referring again to Eq. (3.16), we write the MFT single particle wave functions as

$$\psi^i_\beta(\mathbf{x})\rightarrow\psi^i_{n_\beta l_\beta j_\beta m_\beta}(\mathbf{x})=u^i_{n_\beta l_\beta j_\beta}(x)\mathcal{Y}_{l^{(i)}_\beta j_\beta m_\beta}(\hat{x},\sigma) \tag{B2}$$

where i is a Dirac component index and

$$u^i_\beta(x)=\begin{cases}u_\beta(x) & \text{for } i=1\,,\\ \iota\underline{u}_\beta(x) & \text{for } i=2\end{cases}$$

with u ($\underline{u}$) being the real upper (lower) component bound state radial wave function and where

$$\mathcal{Y}_{l^{(i)}jm}(\hat{x};\sigma)\equiv[Y_{l^{(i)}}(\hat{x})\chi_{1/2}(\sigma)]_{jm}$$

and $l^{(2)}\equiv(2j-l^{(1)})$ that is, $l^{(2)}$ is the "other parity" lower component orbital angular momentum associated with the upper component orbital angular momentum $l^{(1)}$.

The nonspectral MFT single particle propagator[12] has a similar form:

$$\begin{aligned}G^{ij}_{\mathrm{MF}}(\mathbf{x},\mathbf{y};\omega)=\sum_{l'j'm}&[\psi^i_{\mathbf{u};l'j'm}(\mathbf{x};\omega)\bar{\psi}^j_{\mathbf{v};l'j'm}(\mathbf{y};\omega)\theta(y-x)\\ &+\psi^i_{\mathbf{v};l'j'm}(\mathbf{x};\omega)\bar{\psi}^j_{\mathbf{u};l'j'm}(\mathbf{y};\omega)\theta(x-y)]\end{aligned} \tag{B3}$$

where

$$\psi^i_{\mathbf{u};l'j'm}(\mathbf{x};\omega)=\psi^i_{\mathbf{u};l'j'}(x;\omega)\mathcal{Y}_{l'^{(i)}j'm}(\hat{x},\sigma) \tag{B4}$$

with

$$\psi^i_{\mathbf{u};l'j'}(x)=\begin{cases}\mathbf{u}_{l'j'}(x) & \text{for } i=1\\ \iota\underline{\mathbf{u}}_{l'j'}(x) & \text{for } i=2\ ,\end{cases} \tag{B5}$$

$\mathbf{u}$ ($\underline{\mathbf{u}}$) being the upper (lower) component radial wave function for the solution of the MFT Dirac equation [i.e., the MFT version of Eq. (2.4)] at energy ω with regular boundary conditions at $x=0$. For ω above particle threshold, $\mathbf{u}$ and $\underline{\mathbf{u}}$ will be complex. Similarly, $\psi^i_{\mathbf{v};ljm}(\mathbf{x};\omega)$ represents a solution to the MFT Dirac equation which is regular at large distances. In practice, this quantity is obtained by integrating the Dirac equation inward from some large radius (typically 10 fm) at which point $\psi_{\mathbf{v}}$ is matched to the outgoing wave spherical Hankel function $h_l^{(1)}(kx)$ where $k=(\omega^2+2m\omega)^{1/2}$ for $\omega>0$. For $\omega\le 0$, $\psi_{\mathbf{v}}$ is matched to $h_l^{(1)}(\iota\kappa x)$ with $\kappa=(\omega^2-2m\omega)^{1/2}$ where we now specify $\omega=\epsilon-m$, ϵ being the energy appearing in the MFT Dirac equation [Eq. (2.4)].

With these conventions G_{MF} becomes

$$G^{ij}_{\mathrm{MF}}(\mathbf{x},\mathbf{y};\omega)=\sum_{l'j'm} G^{ij}_{l'j'}(x,y;\omega)\times\mathcal{Y}_{l'^{(i)}j'm}(\hat{x},\boldsymbol{\sigma}_x)\mathcal{Y}^{\dagger}_{l'^{(j)}j'm}(\hat{y},\boldsymbol{\sigma}_y) \tag{B6}$$

where

$$G^{ij}_{l'j'}(x,y;\omega)=\psi^i_{\mathbf{u};l'j'}(x;\omega)\bar{\psi}^j_{\mathbf{v};l'j'}(y;\omega)\theta(y-x)+\psi^i_{\mathbf{v};l'j'}(x;\omega)\bar{\psi}^j_{\mathbf{u};l'j'}(y;\omega)\theta(x-y) \tag{B7}$$

and

$$\bar{\psi}^i_{\mathbf{u}}=\begin{cases}\mathbf{u}_{l'j'} & \text{for } i=1\\ +\iota\mathbf{u}_{l'j'} & \text{for } i=2\end{cases} \tag{B8}$$

and similarly for $\bar{\psi}^i_{\mathbf{v}}$. Note that there is no conjugation of the radial functions above. This is consistent with the usual prescription[3] to be used in constructing the single particle propagator in the continuum.

We combine these expressions, couple the $\mathcal{Y}$'s of like arguments together, and use the identity

$$[\mathcal{Y}_{lj}(\hat{x},\boldsymbol{\sigma})\mathcal{Y}^{\dagger}_{l'j'}(\hat{x},\boldsymbol{\sigma})]_{JM}=(-)^{l'}\sum_{LS}[(l\tfrac{1}{2})_j(l'\tfrac{1}{2})_{j'}|(ll')_L(\tfrac{1}{2}\tfrac{1}{2})_S]_J C_{ll'L}[Y_L(\hat{x})(\chi_{1/2}\chi^{\dagger}_{1/2})_S]_{JM} \tag{B9}$$

where $[(l\frac{1}{2})_j(l'\frac{1}{2})_{j'}|(ll')_L(\frac{1}{2}\frac{1}{2})_S]_J$ is a unitary transformation coefficient proportional to a 9-j symbol and

$$C_{ll'L}\equiv\left[\frac{(2l+1)(2l'+1)}{4\pi(2L+1)}\right]^{1/2}(ll'00|L0)\ .$$

We can then write

$$\Pi^{ij;kl}_{\mathrm{MF}}(\mathbf{x},\mathbf{y};\omega)=\sum_{\substack{LL'\\SS'\\JM}}\Pi^{ij;kl}_{LL'SS'J}(x,y;\omega)\{Y_L(\hat{x})[\chi_{1/2}(\boldsymbol{\sigma}_x)\chi^{\dagger}_{1/2}(\boldsymbol{\sigma}_x)]_S\}_{JM}\{Y_{L'}(\hat{y})[\chi_{1/2}(\boldsymbol{\sigma}_y)\chi^{\dagger}_{1/2}(\boldsymbol{\sigma}_y)]_{S'}\}^{\dagger}_{JM} \tag{B10}$$

where

$$\Pi^{ij;kl}_{LL'SS'J}(x,y;\omega)=-\sum_{\substack{F\ge\beta>0\\l'j'}}[\mathcal{A}^{ij}_{l_\beta j_\beta l'j';LSJ}\mathcal{A}^{lk}_{l_\beta j_\beta l'j';L'S'J}u^i_{l_\beta j_\beta}(x)\bar{u}^{\,l}_{l_\beta j_\beta}(y)G^{kj}_{l'j'}(y,x;\epsilon_\beta-\omega)+\mathcal{A}^{ij}_{l'j'l_\beta j_\beta;LSJ}\mathcal{A}^{lk}_{l'j'l_\beta j_\beta;L'S'J}u^k_{l_\beta j_\beta}(y)\bar{u}^{\,j}_{l_\beta j_\beta}(x)G^{il}_{l'j'}(x,y;\epsilon_\beta+\omega)]\ . \tag{B11}$$

with

$$\mathcal{A}^{mn}_{l_1j_1l_2j_2;\Lambda\Sigma J}=(-1)^{l_2^n}C_{l_1^ml_2^n\Lambda}[(l_1^m\tfrac{1}{2})_{j_1}(l_2^n\tfrac{1}{2})_{j_2}|(l_1^ml_2^n)_\Lambda(\tfrac{1}{2}\tfrac{1}{2})_\Sigma]_J\ . \tag{B12}$$

We now consider the "kernel" appearing in Eq. (B1) which connects the two MFT polarization insertions. The vertices are expressed as

$$\begin{aligned}&\Gamma_s\to\iota g_s\to\iota g_s(\Gamma_s)_D\sigma_s,\quad(\Gamma_s)_D=\mathbf{1}_D,\quad\sigma_s=\mathbf{1}_P\\ &\Gamma^0_v\to-\iota g_v\gamma^0\to-\iota g_v(\Gamma^0_v)_D\sigma_{v^0},\quad(\Gamma^0_v)_D=\begin{bmatrix}1&0\\0&-1\end{bmatrix}_D,\quad\sigma_{v^0}=\mathbf{1}_P\\ &\Gamma_v\to\iota g_v\boldsymbol{\gamma}\to-\iota g_v(\Gamma_v)_D\sigma_{\mathbf{v}},\quad(\Gamma_v)_D=\begin{bmatrix}0&1\\-1&0\end{bmatrix}_D,\quad\sigma_{\mathbf{v}}=\boldsymbol{\sigma}_P\end{aligned} \tag{B13}$$

where the subscript D refers to matrices in Dirac component space and P refers to matrices in Pauli spinor space. Then the contribution to the kernel due to meson type N can be written as

$$-\iota g_N^2 \sum_a (\Gamma_N^a)_D^{m'm}(\Gamma_{N;a})_D^{n'n} \sum_{LJM} f_{N;L}(z_1,z_2;\omega)[Y_L(\hat{z}_1)\sigma_{S_a}]_{JM}[Y_L(\hat{z}_2)\sigma_{S_a}]^\dagger_{JM} \tag{B14}$$

where we have used the fact that $D_{N;ab}$ is diagonal in the generalized coordinate indices a and b. Also σ_{S_a} is the Pauli spin operator relevant to meson type N (label suppressed) and coordinate a and $f_{N;L}$ arises from the Slater expansion of D_N. We use the spin-angle identity

$$\int d\hat{x}\, d\sigma \{Y_L(\hat{x})[\chi_{1/2}(\sigma)\chi^\dagger_{1/2}(\sigma)]_S\}^\dagger_{JM}[Y_{L'}(\hat{x})\sigma_{S'}]_{J'M'} = \sqrt{2}\delta_{LL'}\delta_{SS'}\delta_{JJ'}\delta_{MM'} \tag{B15}$$

to perform the integrals over $\hat{z}_1$, $\hat{z}_2$, and the spin variables in Eq. (B1). Equation (B15) implies a separation into partial waves of total angular momentum and parity J^π as expected. The first iteration of the MFT polarization insertion can then be expressed as radial functions times one overall spin-angle factor:

$$-\iota\Pi^{(0+1)ij;kl}_{\rm MF}(\mathbf{x},\mathbf{y};\omega) = \sum_{\substack{LL'\\SS'\\JM}} [-\iota\Pi^{ij;kl}_{LL'SS'J}(x,y;\omega) + B^{ij;kl}_{LL'SS'J}][Y_L(\hat{x})(\chi_{1/2}\chi^\dagger_{1/2})_S]_{JM}[Y_{L'}(\hat{y})(\chi_{1/2}\chi^\dagger_{1/2})_{S'}]^\dagger_{JM} \tag{B16}$$

where

$$B^{ij;kl}_{LL'SS'J} = 2\int z_1^2 dz_1 z_2^2 dz_2 \sum_{\substack{L''\\N,a}} (-\iota)\Pi^{ij;mm'}_{LL''SS_a J}(x,z_1;\omega)(-\iota g_N^2)(\Gamma_N^a)^{m'm}\iota f_{N;L''}(z_1,z_2;\omega)(\Gamma_N;a)^{n'n}(-\iota)\Pi^{nn';kl}_{L''L'S_aS'J}(z_2,y;\omega)\ . \tag{B17}$$

The ring sum is accomplished by letting $\Pi^{(0+1)} \to \Pi_{\rm RPA}$ on the left-hand side of Eq. (B16) and $\Pi_{\rm MF}(z_2,y;\omega) \to \Pi_{\rm RPA}(z_2,y;\omega)$ on the right-hand side of Eq. (B17). The result is the RPA radial equation of Eq. (5.1) where the radial MFT polarization insertion is given by Eqs. (B11) and (B12).

APPENDIX C

The RPA analogue of Eq. (3.3) is

$$\Pi^{ij;kl}_{\rm RPA}(\mathbf{x},\mathbf{y};\omega\to\omega_n+\iota\eta) = -\frac{[\bar{\mathcal{F}}^{(n)}_{\rm RPA}(\mathbf{x})]^{ij}[\mathcal{F}^{(n)}_{\rm RPA}(\mathbf{y})]^{kl}}{\iota\eta} \tag{C1}$$

where ω_n is the RPA excitation energy of the nth excited state and $(\mathcal{F}^{(n)}_{\rm RPA})^{kl}$ is the associated RPA transition density which is a matrix in Dirac component space. The partial-wave expansion of $\Pi_{\rm RPA}$ discussed in Appendix B implies

$$-\iota\eta\Pi^{ij;kl}_{{\rm RPA};LL'SS'J}(x,y;\omega_n+\iota\eta) = [\bar{\mathcal{F}}^{(n)}_{{\rm RPA};LSJ}(x)]^{ij}[\mathcal{F}^{(n)}_{{\rm RPA};L'S'J}(y)]^{kl} \tag{C2}$$

and

$$\mathcal{F}_{LSJM}(\mathbf{y}) = \mathcal{F}_{LSJ}(y)[Y_L(\hat{y})\sigma_S]^\dagger_{JM}\ . \tag{C3}$$

Hence [see Eq. (3.5)] the RPA matrix element of vertex operator $\mathcal{O}$ for this transition is

$$\langle\mathcal{O}\rangle^{(n)}_{\rm RPA} \to \sum_{LSJM}\langle\mathcal{O}_{LSJM}\rangle^{(n)}_{\rm RPA}\ ,$$

where

$$\langle\mathcal{O}_{LSJM}\rangle^{(n)}_{\rm RPA} \equiv \sum_{lk}\int d^2y\, \mathcal{O}^{lk}_{LSJM}(\mathbf{y})[\mathcal{F}^{(n)}_{{\rm RPA};LSJM}(\mathbf{y})]^{kl} \to \sqrt{2}\sum_{lk}\int_0^\infty y^2 dy\ \mathcal{O}^{lk}_{LSJ}(y)[\mathcal{F}^{(n)}_{{\rm RPA};LSJ}(y)]^{kl} \tag{C4}$$

for $\mathcal{O}_{LSJM}(\mathbf{y}) \equiv \mathcal{O}_{LSJ}(y)[Y_L(\hat{y})\sigma_S]_{JM}$.

The RPA transition density may be extracted from the $\Pi_{\rm RPA}$ of Eq. (5.1) via the following procedure. Define

$$\alpha^2 \equiv (-)^{k+l+1}\iota\eta\Pi^{lk;kl}_{{\rm RPA};L'L'S'S'J}(y_0,y_0;\omega_n+\iota\eta) = |[\mathcal{F}^{(n)}_{{\rm RPA};L'S'J}(y_0)]^{kl}|^2$$

which is positive definite. Note that the phase $(-)^{k+l}$ comes from the definition $\bar{\mathcal{F}} \equiv \gamma^0\mathcal{F}^\dagger\gamma^0$. Then

$$-\frac{\iota\eta}{\alpha}\Pi^{ji;kl}_{{\rm RPA};LL'SS'J}(x,y_0;\omega_n+\iota\eta) = [\bar{\mathcal{F}}^{(n)}_{{\rm RPA};LSJ}(x)]^{ji} = (-)^{i+j}\{\mathcal{F}^{(n)}_{{\rm RPA};LSJ}(x)]^{ij}\}^* \tag{C5}$$

which finally yields the radial transition density to be used in, e.g., Eq. (C4).

[1] C. J. Horowitz and B. D. Serot, Nucl. Phys. **A368**, 503 (1981).
[2] B. D. Serot and J. D. Walecka, Adv. Nucl. Phys. **16**, 1 (1986).
[3] D. J. Thouless, Nucl. Phys. **22**, 78 (1961).
[4] A. de Shalit and H. Feshbach, *Theoretical Nuclear Physics* (Wiley, New York, 1978), Vol. 1, and references therein.
[5] J.-P. Blaizot and G. Ripka, *Quantum Theory of Finite Systems* (MIT Press, Cambridge, Mass., 1986), and references therein.
[6] A. Fetter and J. D. Walecka, *Quantum Theory of Many Particle Systems* (McGraw-Hill, New York, 1971), and references therein.

[7]R. J. Furnstahl, Phys. Lett. **152B**, 313 (1985).
[8]R. J. Furnstahl, Phys. Rev. C **38**, 370 (1988).
[9]R. J. Furnstahl and J. Dawson, private communication; and (unpublished).
[10]P. G. Blunden and P. McCorquodale, Phys. Rev. C **38**, 1861 (1988).
[11]K. Wehrberger and F. Beck, Phys. Rev. C **37**, 1148 (1988).
[12]J. R. Shepard, E. Rost, C.-Y. Cheung, and J. A. McNeil, Phys. Rev. C **37**, 1130 (1988).
[13]S. A. Chin, Ann. Phys. (N.Y.) **108**, 301 (1977).
[14]S. Shlomo and G. Bertsch, Nucl. Phys. **A243**, 507 (1975).
[15]S. Iichi, W. Bentz, A. Arima, and T. Suzuki, Phys. Lett. B **192**, 11 (1987).
[16]E. Rost and J. R. Shepard, computer code DRPA, unpublished.
[17]E.g., E. Rost and J. R. Shepard, computer code DRIA, unpublished.
[18]T. N. Buti *et al.*, Phys. Rev. C **33**, 755 (1986).
[19]B. Frois and C. N. Papanicolas, Annu. Rev. Nucl. Part. Sci. **37**, 133 (1987).
[20]J. B. Flanz *et al.*, Phys. Rev. Lett. **41**, 1642 (1978); G. Peterson, private communication.
[21]S. Ichii *et al.*, Nucl. Phys. **A487**, 493 (1988).
[22]C. J. Horowitz, Phys. Lett. B **208**, 8 (1988).
[23]J. R. Shepard *et al.*, Phys. Rev. C **29**, 2243 (1984).
[24]D. J. Rowe and S. S. M. Wong, Nucl. Phys. **A153**, 561 (1970).
[25]J. Heisenberg *et al.*, Nucl. Phys. **A164**, 353 (1971); also P. L. Hallowell *et al.*, Phys. Rev. C **7**, 1396 (1973).
[26]J. E. Wise *et al.*, Phys. Rev. C **31**, 1699 (1985).
[27]C. Hyde-Wright *et al.*, Phys. Rev. C **35**, 880 (1987).
[28]D. B. Holtkamp *et al.*, Phys. Rev. Lett. **45**, 420 (1980).
[29]C. Price and G. E. Walker, Phys. Lett. **155B**, 17 (1985).
[30]J. A. McNeil, R. J. Furnstahl, E. Rost, and J. R. Shepard, Phys. Rev. C **40**, 399 (1989).
[31]J. R. Taylor, *Scattering Theory: The Quantum Theory of Nonrelativistic Collisions* (Krieger, Malabar, Florida, 1983).
[32]J. R. Shepard, D. Oakley, and R. J. Peterson (unpublished).
[33]S. Nishizaki *et al.*, Phys. Lett. B **171**, 1 (1986).
[34]Z. E. Meziani *et al.*, Phys. Rev. Lett. **52**, 2130 (1984).
[35]C. J. Horowitz, Phys. Lett. B **208**, 8 (1988).
[36]T. Suzuki, Phys. Rev. C **37**, 549 (1988).
[37]C. J. Horowitz and J. Piekarewicz, Phys. Rev. Lett. **62**, 391 (1989).
[38]E. Rost and J. R. Shepard, Phys. Rev. C **40**, 1736 (1989).
[39]M. E. Rose, *Relativistic Electron Theory* (Wiley, New York, 1961).